J. Fluid Mech. (2010), *vol.* 648, *pp.* 83–121.
doi:10.1017/S0022112009992904

The energetics of flow through a rapidly oscillating tube. Part 1. General theory

ROBERT J. WHITTAKER[1], SARAH L. WATERS[1], OLIVER E. JENSEN[2], JONATHAN BOYLE[3] AND MATTHIAS HEIL[3]

[1]Oxford Centre for Industrial and Applied Mathematics, University of Oxford, 24–29 St Giles, Oxford OX1 3LB, UK

[2]School of Mathematical Sciences, University of Nottingham, University Park, Nottingham NG7 2RD, UK

[3]School of Mathematics, University of Manchester, Oxford Road, Manchester M13 9PL, UK

(Received 8 December 2008; revised 20 October 2009; accepted 21 October 2009)

We examine the effect of prescribed wall-driven oscillations of a flexible tube of arbitrary cross-section, through which a flow is driven by prescribing either a steady flux at the downstream end or a steady pressure difference between the ends. A large-Womersley-number large-Strouhal-number regime is considered, in which the oscillations of the wall are small in amplitude, but sufficiently rapid to ensure viscous effects are confined to a thin boundary layer. We derive asymptotic expressions for the flow fields and evaluate the energy budget. A general result for the conditions under which there is zero net energy transfer from the flow to the wall is provided. This is presented as a critical inverse Strouhal number (a dimensionless measure of the background flow rate) which is expressed only in terms of the tube geometry, the fluid properties and the profile of the prescribed wall oscillations. Our results identify an essential component of a fundamental mechanism for self-excited oscillations in three-dimensional collapsible tube flows, and enable us to assess how geometric and flow properties affect the stability of the system.

1. Introduction

Flow-induced oscillations of fluid-conveying elastic vessels arise in many engineering and biomechanical systems. Examples include pipe flutter, wheezing during forced expiration from the pulmonary airways and the development of Korotkoff sounds during blood pressure measurement by sphygmomanometry (Heil & Jensen 2003; Grotberg & Jensen 2004).

Experimental studies of flow in collapsible tubes are typically performed with the Starling resistor shown in figure 1. A finite-length elastic tube is mounted on two rigid tubes and flow is driven through the system either by imposing the flow rate (using a volumetric pump) or by applying a fixed pressure drop between the far-upstream and far-downstream ends of the two rigid tubes. The collapsible segment is contained inside a pressure chamber which allows the external pressure acting on the elastic tube to be controlled independently of the fluid pressure. If the transmural (internal minus external) pressure becomes sufficiently negative, the elastic tube buckles non-axisymmetrically. Once buckled, the tube is very flexible and, as a result, small

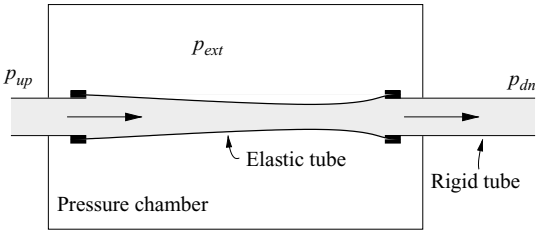

FIGURE 1. The typical experimental set-up, known as a 'Starling resistor', which comprises an elastic tube clamped between rigid supports, surrounded by an outer pressure chamber. Flow is driven through the tube from left to right by an applied pressure difference $p_{up} - p_{dn}$ between the two ends. Alternatively, a volumetric pump may be used to set a specific flux at one end or the other. The pressure p_{ext} in the surrounding chamber can be adjusted to control the degree of collapse of the elastic tube.

changes in transmural pressure can induce large changes in the tube shape, resulting in strong fluid–structure interaction. Experiments show that the elastic tube segment has a propensity to develop large-amplitude self-excited oscillations of great complexity when the flow rate is increased beyond a certain value (Bertram 2003).

The mechanisms responsible for the development of these self-excited oscillations are still not fully understood. Early theoretical analyses of flow in collapsible tubes (reviewed, for example, in Heil & Jensen 2003) were based on spatially one-dimensional models. These invariably required numerous *ad hoc* assumptions to model the complicated three-dimensional wall mechanics, the viscous losses, the effect of flow separation, etc. within the framework of the cross-sectionally averaged equations. As a first step towards a more rational theoretical approach to the problem, Jensen & Heil (2003) analysed the development of self-excited oscillations in a two-dimensional channel in which part of one of the rigid walls is replaced by a tensioned membrane. This set-up is attractive because it can, at least in principle, be realized experimentally but avoids many of the complexities of the full three-dimensional system. Luo & Pedley (1996) had previously simulated nonlinear self-excited oscillations in this system using a finite-element method, although a rational theoretical analysis of these oscillations was (and still is) lacking.

Jensen & Heil (2003) analysed this system in a parameter regime in which the wall stiffness (or pre-stress) is sufficiently large that the wall performs high-frequency oscillations. In this regime the oscillatory fluid flow induced by the wall motion has a two-region structure: an inviscid core flow region, surrounded by thin Stokes layers near the channel walls. Conservation of volume implies that, during phases when the wall moves inward, some of the fluid in the collapsible section must be displaced into the upstream and downstream rigid channels. The oscillatory wall motion therefore generates axial sloshing flows that increase (decrease) the volume flux in the downstream rigid section while decreasing (increasing) the volume flux in the upstream rigid section when the wall moves inward (outward). Jensen & Heil (2003) showed that the interaction between the wall-driven oscillatory axial sloshing flow and the mean flow through the tube allows the wall to extract energy from the flow if the magnitude of the sloshing flows in the upstream rigid channel exceeds sufficiently that in the downstream section. Theoretical predictions for the flow rate at which self-excited oscillations develop were found to be in excellent agreement with direct numerical simulations (based on the solution of the unsteady two-dimensional

Navier–Stokes equations, fully coupled to a beam-theory model of the elastic channel wall). Furthermore, the flow features predicted by the small-amplitude analysis were found to provide an excellent description of the system's behaviour during the large-amplitude limit-cycle oscillations that developed subsequently.

Jensen & Heil (2003) provided an explanation of the instability mechanism in terms of the fluid's energy balance, given by (2.12) below. Briefly, the energy fluxes into and out of the system are the kinetic energy flux through the tube ends, the work done by pressure and viscous forces at the tube ends and at the wall, and the losses due to dissipation. Any net energy flux into the system necessarily alters the total (kinetic) energy content of the system. If an instability is to grow, the total energy of the system needs to increase, on average, over time, so the net time-averaged flux into the system must be positive. By virtue of a non-zero time-mean square, any oscillatory flow at the upstream end increases the kinetic energy influx, and any oscillatory flow at the downstream end increases the kinetic energy outflux. If the amplitude of the oscillatory flow is greater at the upstream end, then there will be a net increase in kinetic energy flux. If this increase is greater than the additional dissipative (or other) losses, then there is energy available to drive an instability.

When assessing the applicability of this instability mechanism to three-dimensional flows in collapsible tubes, Heil & Waters (2006) showed that, while the mechanism is, in principle, independent of the spatial dimension, the sloshing flows generated by small-amplitude non-axisymmetric oscillations of circular cylindrical tubes are much weaker than those generated in the corresponding two-dimensional system. In a two-dimensional channel, a transverse wall deflection of amplitude Δ generates an $O(\Delta)$ sloshing flow. However, the preferred mode of buckling for a cylindrical tube typically has an azimuthal wavenumber of 2 and very nearly preserves circumferential length. A small-amplitude non-axisymmetric buckling deformation of this form preserves cross-sectional area at leading order, and hence deformations of $O(\Delta)$ only generate axial sloshing flows of size $O(\Delta^2)$. The net influx of kinetic energy due to these sloshing flows is therefore much smaller in three dimensions than in two dimensions. Heil & Waters (2006) showed that the flows generated by high-frequency, oscillatory, non-axisymmetric wall deflections of a circular cylindrical tube of moderate length are, in fact, dominated by the transverse flows within the tube's cross-sections. In the regime they studied, the interaction with the mean flow is too weak to extract sufficient energy from it.

The magnitude of the sloshing flows can, however, be increased either by making the tube sufficiently long ($O(\Delta)$ non-axisymmetric wall deflections inducing $O(\Delta^2)$ area changes applied over an axial length of $O(1/\Delta)$ generate $O(\Delta)$ sloshing flows), or if the tube wall performs oscillations about a sufficiently non-axisymmetric mean configuration. The latter possibility was explored by Heil & Waters (2008), who analysed the energy budget of flows through rapidly oscillating tubes whose wall motion was prescribed. They demonstrated that, if the tube wall performs oscillations about a non-axisymmetrically buckled mean configuration, the wall begins to extract energy from the viscous mean flow when the flow rate exceeds a certain threshold. Heil & Waters (2008) conjectured that, in a problem with full fluid–structure interaction, this flow rate corresponds to the threshold beyond which the amplitude of the wall oscillations would grow. Numerical simulations were employed to determine the dependence of the critical flow rate (expressed as a critical inverse Strouhal number) on the Womersley number of the flow, and a scaling argument was

presented to explain the observed simple functional relationship between these two quantities.

The asymptotic analysis of Heil & Waters (2008) was restricted to tubes whose initial configuration was a small deformation of a circular cylinder. In this paper, we extend the work of Heil & Waters to tubes of arbitrary initial shape, with the proviso that the cross-sections vary only slowly axially. We consider a particular asymptotic regime, corresponding to long-wavelength small-amplitude high-frequency oscillations. This regime corresponds to a region of parameter space where the instability first identified by Jensen & Heil (2003) should occur.

As in Heil & Waters (2008), we consider prescribed periodic wall motions, rather than the full fluid–structure interaction (FSI) problem. In the FSI problem, the stability of the system can be judged by the increase (or decrease) of the total kinetic and elastic energy of the fluid and the tube wall over time. If an instability grows, then the energy budget of the fluid must show a gradual increase in kinetic energy content, and also (on average) a net flux of energy to the tube wall in order to increase the latter's kinetic and elastic energy. In the forced problem there is no notion of kinetic and elastic energy in the wall, and the kinetic energy of the fluid is necessarily constant when averaged over a period of the fixed-amplitude oscillations. Instead we consider the energy transfer to and from the forcing mechanism, i.e. the work done by the fluid on the wall. If this work is positive when integrated over a period, then the system is able to extract energy from the mean flow to sustain the oscillations and has a surplus of energy that could potentially drive a growing instability were the forcing removed. If this work is negative, then the forcing is putting energy into the system to sustain the oscillations. We conjecture that in such cases the oscillations would decay were the forcing to be removed.

The response to forced oscillations is also relevant to the study of non-peristaltic valveless pumps, where an oscillatory forcing of an elastic section of a tube is used to induce a mean flow along the tube (Liebau 1954). Such pumps do not rely on volume changes to directly pump the fluid, but instead generate a pressure gradient from the interaction of waves generated by the forcing. This mechanism may be present in the foetal circulatory system and also has industrial and biotechnological applications. Recent experimental and theoretical work has been reported by Hickerson, Rinderknecht & Gharib (2005), Hickerson & Gharib (2006), Bringley *et al*. (2008) and Avrahami & Gharib (2008).

The present study also overlaps with a large body of work on the stability of flow through tubes and channels subject to external perturbations, such as transverse or normal wall oscillation (e.g. Floryan, Szumbarski & Wu 2002; Jovanovic 2008), a body force (Jovanovic & Bamieh 2005), wall blowing or suction (Gao & Lu 2006), or wall disturbances of prescribed shape (e.g. Szumbarski & Floryan 2006). Such stability calculations generally involve the solution of forced linear systems, for which the response is assessed via analysis of the excitation (or suppression) of intrinsic local modes. Such modes might display transient or exponential growth and, in extended systems, exhibit absolute or convective instability. Thus, in a two-dimensional channel, Tollmien–Schlichting (vorticity) waves are the dominant response to a localized oscillating wall indentation of the appropriate frequency (Pedley & Stephanoff 1985; Ralph & Pedley 1988). Alternatively in a three-dimensional channel, a stationary wall perturbation can generate streamwise vortices (Floryan 2003). We do not address such local receptivity questions here, however. Instead, we focus on the global inhomogeneous solution of the forced linear problem, constructing an asymptotic solution in a parameter regime that does not capture any unstable hydrodynamic

modes. Extending our description of the forced solution into the weakly nonlinear regime, and taking full account of boundary conditions at either end of the tube, we investigate whether the forcing does net work on the system, or acts as an energy sink. As explained above, this is an important precursor to understanding the global instability of experimental systems such as the Starling Resistor.

In what follows, we derive an asymptotic solution for the fluid flow and pressure fields in response to the imposed oscillations, and also determine the criticality condition for zero time-averaged energy transfer to the wall (see (9.5)). The latter is presented as a critical inverse Strouhal number (a dimensionless measure of the background flow rate) given in terms of the other problem parameters and variables. The expression is a relatively simple combination of the fluid properties and a set of integrals involving the geometry of the tube and the prescribed oscillations.

This paper is organized as follows. In § 2 we give a mathematical description of the problem to be solved, along with the scalings and parameter regime of interest. In § 3 we consider the solution structure and decompose the pressure and velocity into (temporal) frequency components. In §§ 4–7 we present a general solution to the problem as a power series expansion in a pair of small parameters ϵ (encapsulating the size of the Strouhal number, Womersley number and aspect ratio) and δ (encapsulating the amplitude of the oscillations). The energy budget is examined in detail in § 8. The main result of the paper, equation (9.5), is presented and interpreted in § 9. Discussion and concluding remarks are presented in § 10. In Part 2 of this work (Whittaker *et al.* 2010) we present a comparison of the theoretical results derived here with numerical simulations.

2. Set-up and governing equations

2.1. *Problem description*

As shown in figure 2, we consider a tube of length L and typical diameter $2a$, where $a \ll L$. The tube is filled with fluid of density ρ and dynamic viscosity μ. The cross-sectional shape and area may vary along the length of the tube, but we assume that such variations occur over the length scale L, so the gradients are at most $O(L^{-1})$. The precise definition of a is left open, since sensible choices will depend on the problem at hand. Possibilities include the radius of an equivalent circular cylinder with the same volume or surface area as the undeformed tube, or the radius of an equivalent circle that matches the perimeter or area at one end of the tube.

Portions of the tube adjacent to each end may be considered rigid and so unable to move, as in the typical experimental set-up (see figure 1). However, since we are considering prescribed deformations only, this arrangement needs no special treatment. It is simpler to consider the general case in which the whole tube *can* undergo deformations, and then set the deformations to be zero in any desired sections. The only restrictions we need to impose are that surface remains sufficiently smooth (including at joints between any rigid and flexible sections), and that the ends of the tube remain fixed with a fixed gradient (which is automatically satisfied if there are rigid end sections). The tube wall undergoes prescribed oscillations of frequency ω and typical amplitude $a\Delta$ about what we shall term the *steady configuration*. The oscillations are assumed to be of small amplitude ($\Delta \ll 1$) but sufficiently high frequency for the induced oscillatory axial velocities to be significant. The oscillations must be harmonic with a single frequency ω, but the phase of the wall displacement may vary with spatial position, thus allowing a variety of axial and azimuthal mode shapes to be considered.

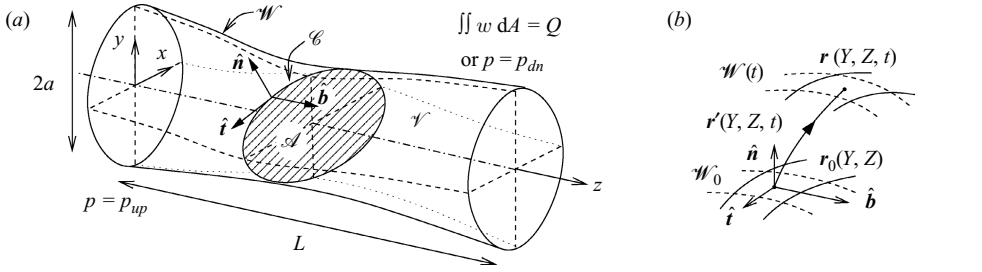

FIGURE 2. (*a*) A sketch of the flexible tube showing the coordinates, dimensions and notation for the various surfaces and volumes. The centreline lies along $x = y = 0$, with z being the axial coordinate. The mean flow is from left to right, with a pressure boundary condition at the upstream end, and either a flux boundary condition or a second pressure condition at the downstream end. (*b*) A close-up of the upper surface of the tube depicting the triad of unit vectors $(\hat{\boldsymbol{n}}, \hat{\boldsymbol{t}}, \hat{\boldsymbol{b}})$ aligned with the surface $\mathscr{W}_0$ in the steady configuration and the displacement vector $\boldsymbol{r}' = \boldsymbol{r} - \boldsymbol{r}_0$.

A mean flow is driven along the length of the tube in response to either a prescribed volume flux at one end or a prescribed pressure drop between the two ends. We denote by Q the steady volume flux of the background flow that would occur with the same boundary conditions in the absence of any oscillations. If a flux boundary condition is used, Q is simply the prescribed flux. In the case where we prescribe the pressure drop, Q must be computed by solving a steady flow problem.

Finally, we assume that the flow remains laminar at all times and that the viscous boundary layers remain attached to the tube walls. These assumptions are reasonable provided that the Reynolds number

$$Re = \frac{\rho Q}{\pi \mu a} \tag{2.1}$$

for the background flow is not too large, that the cross-section does not diverge too rapidly in the direction of the flow along the tube and that Δ remains small.

2.2. *Tube geometry and coordinates*

As shown in figure 2, we use z as the axial coordinate, with Cartesian coordinates x and y occupying the transverse planes. The unit axial vector is $\hat{\boldsymbol{z}}$, and we denote transverse components of vectors (i.e. perpendicular to $\hat{\boldsymbol{z}}$) by the symbol '$\perp$'.

The tube wall $\mathscr{W}$ is parameterized by a pair of material surface coordinates (Y, Z). We take $Z = z$, and choose Y to be orthogonal to Z in the steady configuration. The position of the wall at point (Y, Z) is given by $\boldsymbol{r}_0(Y, Z)$ in the steady configuration. The time-dependent deformations are then described by a vector function $\boldsymbol{r}'(Y, Z, t)$, so that the wall element (Y, Z) is located at

$$\boldsymbol{r} = \boldsymbol{r}_0(Y, Z) + \boldsymbol{r}'(Y, Z, t) \tag{2.2}$$

at time t. The conditions in § 2.1 on the motion at the tube ends imply that

$$\boldsymbol{r}' = \boldsymbol{0} \quad \text{and} \quad \hat{\boldsymbol{n}} \cdot \frac{\partial \boldsymbol{r}'}{\partial Z} = 0 \quad \text{at} \quad Z = 0, L, \tag{2.3a,b}$$

where $\hat{\boldsymbol{n}}$ is the normal to the tube wall.

We denote the space enclosed by the tube at time t by $\mathscr{V}(t) \subset \mathbb{R}^3$, and the cross-section by $\mathscr{A}(z, t) \subset \mathbb{R}^2$. The area of the cross-section $\mathscr{A}(z, t)$ is given by $A(z, t)$, and its boundary at the tube wall by $\mathscr{C}(z, t)$. A subscript '0' is used to denote the

corresponding regions in the steady configuration. The boundary $\partial\mathscr{V}$ of the flow domain comprises the tube ends $\mathscr{A}(0,t)=\mathscr{A}_0(0)$ and $\mathscr{A}(L,t)=\mathscr{A}_0(L)$, together with the flexible wall $\mathscr{W}(t)$.

For each point (Y, Z), we introduce a right-handed orthogonal triad of unit vectors $(\hat{\boldsymbol{n}}, \hat{\boldsymbol{t}}, \hat{\boldsymbol{b}})$ aligned with the steady configuration $\mathscr{W}_0$ of the tube wall. The vector $\hat{\boldsymbol{n}}$ is the outward-pointing normal, while $\hat{\boldsymbol{t}}$ and $\hat{\boldsymbol{b}}$ correspond to the coordinates Y and Z as shown in figure 2. From the definition of Y and Z above, we have $\hat{\boldsymbol{t}}\cdot\hat{\boldsymbol{z}}=0$, so $\hat{\boldsymbol{t}}$ lies in the cross-sectional plane.

The unit vectors are linked to the in-plane coordinates by

$$\frac{\partial \boldsymbol{r}_0}{\partial Y} = H_Y^{\mathrm{s}}(Y,Z)\,\hat{\boldsymbol{t}}, \quad \frac{\partial \boldsymbol{r}_0}{\partial Z} = H_Z^{\mathrm{s}}(Y,Z)\,\hat{\boldsymbol{b}}, \tag{2.4a,b}$$

where H_Y^{s} and H_Z^{s} are the appropriate scale factors on the surface. These scale factors can be used to express a surface element $\mathrm{d}S$ in terms of the product $\mathrm{d}Y\,\mathrm{d}Z$ of the surface coordinates, thus

$$\mathrm{d}S = H_Y^{\mathrm{s}}\,H_Z^{\mathrm{s}}\,\mathrm{d}Y\,\mathrm{d}Z. \tag{2.5}$$

We also define four curvatures: K_Y, K_Z, Γ_Y and Γ_Z. These describe how (in the steady configuration) lines on the surface with constant Y or Z bend along their length. They are defined in terms of derivatives of the unit vectors, thus

$$\frac{\partial \hat{\boldsymbol{t}}}{\partial Y} = -K_Y\hat{\boldsymbol{n}} - \Gamma_Y\hat{\boldsymbol{b}}, \quad \frac{\partial \hat{\boldsymbol{b}}}{\partial Z} = -K_Z\hat{\boldsymbol{n}} - \Gamma_Z\hat{\boldsymbol{t}}. \tag{2.6a,b}$$

As a consequence, we also have

$$\frac{\partial \hat{\boldsymbol{n}}}{\partial Y} = K_Y\hat{\boldsymbol{t}}, \quad \frac{\partial \hat{\boldsymbol{n}}}{\partial Z} = K_Z\hat{\boldsymbol{b}}, \quad \frac{\partial \hat{\boldsymbol{b}}}{\partial Y} = \Gamma_Y\hat{\boldsymbol{t}}, \quad \frac{\partial \hat{\boldsymbol{t}}}{\partial Z} = \Gamma_Z\hat{\boldsymbol{b}}. \tag{2.7a–d}$$

These curvatures will be important when it comes to considering a boundary-layer coordinate system and the corresponding equations in § 3.2 and Appendix A.

2.3. *Governing equations and boundary conditions*

To describe the fluid flow, we use the Navier–Stokes equations for a homogeneous incompressible Newtonian fluid. For a total velocity $\boldsymbol{u}\equiv\boldsymbol{u}^{\perp}+w\hat{\boldsymbol{z}}$ and pressure p, we have that

$$\nabla\cdot\boldsymbol{u} = 0, \tag{2.8a}$$

$$\rho\left(\frac{\partial \boldsymbol{u}}{\partial t} + (\boldsymbol{u}\cdot\nabla)\,\boldsymbol{u}\right) = -\nabla p + \mu\nabla^2\boldsymbol{u}. \tag{2.8b}$$

The boundary conditions are as follows. We have no-slip on the (moving) tube walls, i.e.

$$\boldsymbol{u} = \frac{\partial \boldsymbol{r}'}{\partial t} \quad \text{on } \mathscr{W}. \tag{2.9}$$

A flux condition may be applied at one of the tube ends. By definition, this flux is Q, so we have

$$\iint_{\mathscr{A}} w\,\mathrm{d}A = Q \quad \text{at} \quad z=0 \quad \text{or} \quad z=L. \tag{2.10}$$

Alternatively, we may apply a pressure condition at one or both ends, namely

$$p = p_{up} \quad \text{at} \quad z=0 \quad \text{or} \quad p = p_{dn} \quad \text{at} \quad z=L. \tag{2.11a,b}$$

(Formally, these boundary conditions result in an underspecified problem. In the numerical simulations described in Part 2 of this work (Whittaker *et al.* 2010), we apply a specific flow profile for the flux condition and specify parallel flow in addition to the pressure conditions. However, for the long-wavelength asymptotics considered here, the conditions stated above are sufficient.)

Under the mechanism outlined in the introduction, the instability we are examining here cannot occur with a flux condition at the upstream end. This is because there would be no time-averaged kinetic energy influx from the oscillatory flow at the upstream end and the corresponding contribution from the downstream end is always negative. (However, see § 10 for a discussion of other instabilities that may be present.) We therefore consider just two cases: a pressure condition at the upstream end, with either a pressure or a flux condition at the downstream end.

An energy equation may be derived from (2.8) by contracting the momentum equation with $\boldsymbol{u}$ and integrating over $\mathscr{V}(t)$. We obtain

$$\frac{\mathrm{d}}{\mathrm{d}t}\iiint_{\mathscr{V}}\frac{1}{2}\rho|\boldsymbol{u}|^2\,\mathrm{d}V = -\iint_{\partial\mathscr{V}}\frac{1}{2}\rho|\boldsymbol{u}|^2(\boldsymbol{u}-\boldsymbol{v}_b)\cdot\hat{\boldsymbol{N}}\,\mathrm{d}S + \iint_{\partial\mathscr{V}}\boldsymbol{u}\cdot(-p\boldsymbol{I}+2\mu\boldsymbol{e})\cdot\hat{\boldsymbol{N}}\,\mathrm{d}S - \iiint_{\mathscr{V}}2\mu\,\boldsymbol{e}:\boldsymbol{e}\,\mathrm{d}V, \quad (2.12)$$

where $[\boldsymbol{e}]_{ij}=(\nabla_i u_j+\nabla_j u_i)/2$ is the rate-of-strain tensor, $\boldsymbol{I}$ is the identity tensor, $\boldsymbol{v}_b$ is the velocity of the boundary $\partial\mathscr{V}$ of $\mathscr{V}$ ($\boldsymbol{v}_b=0$ at the fixed tube ends), and $\hat{\boldsymbol{N}}$ is the (time-dependent) outward normal at the boundary. Physically, (2.12) states that the rate of change in kinetic energy in $\mathscr{V}$ is equal to the flux of kinetic energy across the boundary, plus the rate of working of the boundary against the fluid pressure and viscous forces, minus the energy lost through viscous dissipation.

2.4. *Non-dimensionalization*

We non-dimensionalize the variables in the problem as follows, with breve accents used to denote the non-dimensional versions. We scale lengths with the tube dimensions, writing:

$$x=a\breve{x},\quad y=a\breve{y},\quad z=L\breve{z},\quad Y=a\breve{Y},\quad Z=L\breve{Z}. \quad (2.13a\text{–}e)$$

We also introduce a dimensionless position vector

$$\breve{\boldsymbol{r}}=\breve{x}\hat{\boldsymbol{x}}+\breve{y}\hat{\boldsymbol{y}}+\frac{L}{a}\breve{z}\hat{\boldsymbol{z}}, \quad (2.14)$$

a dimensionless wall displacement

$$\breve{\boldsymbol{r}}'=\frac{1}{a}\boldsymbol{r}', \quad (2.15)$$

and a dimensionless gradient operator

$$\breve{\nabla}\equiv\breve{\nabla}_{\perp}+\hat{\boldsymbol{z}}\frac{a}{L}\frac{\partial}{\partial\breve{z}}\equiv\left(\hat{\boldsymbol{x}}\frac{\partial}{\partial\breve{x}}+\hat{\boldsymbol{y}}\frac{\partial}{\partial\breve{y}}\right)+\hat{\boldsymbol{z}}\frac{a}{L}\frac{\partial}{\partial\breve{z}}. \quad (2.16)$$

Time and frequencies are non-dimensionalized using a time scale T corresponding to the oscillation period:

$$t=T\breve{t},\quad \omega=T^{-1}\breve{\omega}. \quad (2.17a,b)$$

We leave T arbitrary, rather than simply making the obvious choice $T=2\pi/\omega$, to allow for easier comparisons with the case of free oscillations where the exact frequency is not known in advance.

We non-dimensionalize the axial velocity w with the velocity scale $\mathscr{U}$ of the background flow. For the case of pressure–flux boundary conditions, we define

$$\mathscr{U} = \frac{Q}{\pi a^2}. \tag{2.18a}$$

For the case of pressure–pressure boundary conditions, we choose the scale based on the viscous resistance, and define

$$\mathscr{U} = \frac{ka^2}{\mu L}(p_{up} - p_{dn}), \tag{2.18b}$$

where k is a dimensionless $O(1)$ conductivity factor that it may be convenient to introduce in specific geometries. (For example, with a uniform circular cross-section, choosing $k = 1/8$ sets $\mathscr{U}$ to be the cross-sectional average of the axial Poiseuille flow.)

The slender geometry of the tube dictates different scales for the axial and transverse velocity components. Motivated by the continuity equation, we write

$$\breve{\boldsymbol{u}} \equiv \breve{\boldsymbol{u}}^{\perp} + \frac{L}{a}\breve{w}\hat{\boldsymbol{z}}, \quad \text{where} \quad \boldsymbol{u}^{\perp} = \frac{a\mathscr{U}}{L}\breve{\boldsymbol{u}}^{\perp}, \quad w = \mathscr{U}\breve{w}. \tag{2.19a–c}$$

We scale the pressure on the oscillatory inertial scale, and use p_{up} as the reference pressure. We therefore write

$$p - p_{up} = \frac{\rho L \mathscr{U}}{T}\breve{p}. \tag{2.20}$$

With this non-dimensionalization, (2.8) becomes

$$\breve{\nabla}\cdot\breve{\boldsymbol{u}} \equiv \breve{\nabla}_{\perp}\cdot\breve{\boldsymbol{u}}^{\perp} + \frac{\partial \breve{w}}{\partial \breve{z}} = 0, \tag{2.21a}$$

$$\frac{\partial \breve{\boldsymbol{u}}^{\perp}}{\partial \breve{t}} + \frac{1}{\ell St}(\breve{\boldsymbol{u}}\cdot\breve{\nabla})\breve{\boldsymbol{u}}^{\perp} = -\ell^2\breve{\nabla}_{\perp}\breve{p} + \frac{1}{\alpha^2}\left(\breve{\nabla}_{\perp}^2 + \frac{1}{\ell^2}\frac{\partial^2}{\partial \breve{z}^2}\right)\breve{\boldsymbol{u}}^{\perp}, \tag{2.21b}$$

$$\frac{\partial \breve{w}}{\partial \breve{t}} + \frac{1}{\ell St}(\breve{\boldsymbol{u}}\cdot\breve{\nabla})\breve{w} = -\frac{\partial \breve{p}}{\partial \breve{z}} + \frac{1}{\alpha^2}\left(\breve{\nabla}_{\perp}^2 + \frac{1}{\ell^2}\frac{\partial^2}{\partial \breve{z}^2}\right)\breve{w}, \tag{2.21c}$$

where we have introduced the dimensionless groups

$$St = \frac{a}{\mathscr{U}T}, \qquad \alpha^2 = \frac{\rho a^2}{\mu T}, \qquad \ell = \frac{L}{a}. \tag{2.22a–c}$$

The Strouhal number St gives a ratio of the velocity induced by the wall motion to the velocity of the background flow and also the relative importance of nonlinear inertia. The Womersley number α^2 compares the time scale for viscous diffusion with that of the prescribed wall motion and appears in the equations as an unsteady Reynolds number. The aspect ratio ℓ relates the length to the width of the tube.

The upstream pressure condition (2.11a) becomes

$$\breve{p} = 0 \quad \text{at} \quad \breve{z} = 0, \tag{2.23a}$$

while for the downstream condition, we employ either (2.10) or (2.11b), leading to either

$$\iint_{\mathscr{A}(L)} \breve{w}\,\mathrm{d}A = \pi \quad \text{or} \quad \breve{p} = -\frac{1}{k\alpha^2} \quad \text{at} \quad \breve{z} = 1. \tag{2.23b,c}$$

The displacement of the boundary is written in terms of the non-dimensional complex-valued variables (ξ, η, ζ), all functions of $\check{Y}$ and $\check{Z}$, as

$$\check{\boldsymbol{r}}' = \Delta\,\mathrm{Re}[(\xi\hat{\boldsymbol{n}} + \eta\hat{\boldsymbol{t}} + \ell^{-1}\zeta\hat{\boldsymbol{b}})\mathrm{e}^{\mathrm{i}\check{\omega}\check{t}}]. \tag{2.24}$$

The magnitude of (ξ, η, ζ) determines the amplitude of the oscillations at each point $(\check{Y}, \check{Z})$ on the surface, while the argument determines the phase. Different points can have different amplitudes and phases, allowing a variety of different deformation modes to be considered. In particular, there is no restriction that the wall motion must be entirely in phase, nor that it takes an axial mode-1 form (i.e. that it has a single extremum in displacement amplitude along the length of the tube).

We take each of $|\xi|, |\eta|, |\zeta|$ to be $O(1)$, so that the magnitude of the normal and transverse displacements is $O(a\Delta)$ as assumed. The axial displacements are restricted to a smaller $O(a\Delta/\ell)$ amplitude, to reflect the typical physical response of an elastic tube to slowly axially varying forces in the given slender geometry.

In terms of the dimensionless displacements, the conditions (2.3) at the tube ends require that

$$\xi = \eta = \zeta = \frac{\partial \xi}{\partial \check{Z}} = 0 \quad \text{at} \quad \check{z} = 0 \quad \text{and} \quad \check{z} = 1. \tag{2.25}$$

The curvatures of the surface coordinates introduced in (2.6) are non-dimensionalized as

$$K_Y = \frac{1}{a}\check{K}_Y, \quad K_Z = \frac{a}{L^2}\check{K}_Z, \quad \Gamma_Y = \frac{1}{L}\check{\Gamma}_Y, \quad \Gamma_Z = \frac{a}{L^2}\check{\Gamma}_Z, \tag{2.26a–d}$$

where the scales and geometric factors are chosen so that the non-dimensional curvatures are expected to be $O(1)$ for general a and L.

2.5. *Scaling*

The problem contains several large and small parameters. To exploit this in our analysis we must first assess their relative sizes. For this purpose we introduce a small parameter ϵ that controls the size of these terms and consider the distinguished limit in which $\alpha = O(\epsilon^{-1})$, $\ell = O(\epsilon^{-1/2})$ and $St = O(\epsilon^{-1/2})$, corresponding to

$$\ell St \sim \alpha \sim \ell^2 \gg 1. \tag{2.27}$$

Furthermore, we shall assume that $\Delta \ll \epsilon$, $\Delta = \epsilon\delta$ where δ is another small parameter. These scalings are motivated as follows.

A large Womersley number α^2 in (2.21) means that viscous effects are confined to thin boundary layers (of thickness $O(a/\alpha)$) on the walls and that the flow in the core of the tube is essentially inviscid. This both simplifies the analysis and reduces viscous dissipation (which increases the energy available for possible transfer from the flow to the wall). We make the arbitrary choice $\alpha \sim \epsilon^{-1}$.

The Strouhal number St gives the relative importance of the nonlinear inertia terms to the unsteady ones. Its scaling with ϵ is motivated by the instability mechanism discussed in the introduction. Near marginal stability, the additional kinetic energy flux F due to the oscillatory flow at the tube ends will be of the same order of magnitude as the dissipative losses D from the oscillatory flow in the Stokes layer (see (2.12)). The wall motion forces a transverse oscillatory velocity of $O(a\Delta/T)$, which leads to an axial oscillatory velocity of $O(L\Delta/T)$. The kinetic energy flux through the tube ends scales like the cube of the total axial velocity. Only terms containing even powers of oscillatory quantities have a non-zero contribution when time averaged. The additional mean energy flux due to oscillatory velocity is therefore estimated to

be

$$F \sim \rho \mathscr{U} \left(\frac{L\Delta}{T} \right)^2 a^2 = \rho a^2 \mathscr{U}^3 \cdot \Delta^2 (\ell St)^2. \tag{2.28}$$

The viscous dissipation is dominated by the gradient of the axial oscillatory velocity in the Stokes layer of width $a\alpha^{-1}$, so we estimate

$$D \sim \mu \left(\frac{L\Delta}{T} \frac{\alpha}{a} \right)^2 \frac{a^2 L}{\alpha} \sim \rho a^2 \mathscr{U}^3 \cdot \Delta^2 \frac{(\ell St)^3}{\alpha}. \tag{2.29}$$

The balance $F \sim D$ then yields $\ell St \sim \alpha \sim \epsilon^{-1}$. It is convenient that this balance results in $\ell St \gg 1$, as this means that the nonlinear terms are absent from the problem at leading order; see (2.21).

The large aspect ratio ℓ is largely a mathematical convenience to allow long-wavelength approximations to be used in the analysis. We take the smallest scaling for ℓ that allows these simplifications to be used effectively. This turns out to be $\ell \sim \epsilon^{-1/2}$.

The scaling for Δ ensures that the oscillation amplitude is much less than the $O(a/\alpha)$ thickness of the Stokes boundary layer, which in turn enables the linearization of the boundary conditions. The representation $\Delta = \epsilon\delta$ is found to be convenient in the analysis that follows.

Finally, we note at this point that the Reynolds number (2.1) for the background flow is given by

$$Re = \frac{\rho \mathscr{U} a}{\mu} = \frac{\alpha^2}{St} \sim \epsilon^{-3/2}. \tag{2.30}$$

The above scalings therefore ensure that we are in a high-Reynolds-number regime.

For the case of pressure–pressure boundary conditions, we also introduce the added restriction $\delta^2 \leqslant \epsilon$. As we shall see in § 7, this condition is required to ensure that an additional axial flow driven by the oscillations is no larger than the original background mean flow.

To facilitate the application of these scalings we rewrite the three dimensionless groups introduced in (2.22) in terms of three new parameters R, λ and β, which are all assumed to be $O(1)$ as $\epsilon \to 0$. We then have

$$\ell St = \frac{\lambda}{\epsilon} \gg 1, \quad \alpha^2 = \frac{R^2}{\epsilon^2} \gg 1, \quad \ell = \frac{1}{(\epsilon\beta)^{1/2}} \gg 1, \quad \Delta = \epsilon\delta \ll 1. \tag{2.31a–d}$$

Use of this notation in the subsequent analysis allows the physical origin of each term to be seen more clearly (from the combinations of λ, R and β present) and also makes it easier to see the effect of varying each of the dimensionless groups independently. (Note that any one of λ, R and β could be set equal to unity without loss of generality, via a judicious choice of ϵ.)

2.6. *Tube geometry and normals*

Since we typically decompose vectors into components parallel and perpendicular to the $\hat{\boldsymbol{z}}$ axis, it is convenient to do the same with the surface normal $\hat{\boldsymbol{n}}$. We write

$$\hat{\boldsymbol{n}} = \frac{1}{H_Z^s} \hat{\boldsymbol{n}}^\perp + \frac{G}{\ell} \hat{\boldsymbol{z}}, \tag{2.32}$$

where $G = \ell(\hat{\boldsymbol{n}} \cdot \hat{\boldsymbol{z}})$ is an $O(1)$ measure of the (necessarily small) slope of the tube wall, and $\hat{\boldsymbol{n}}^\perp$ is a unit vector in the plane of the cross-section (and hence satisfies

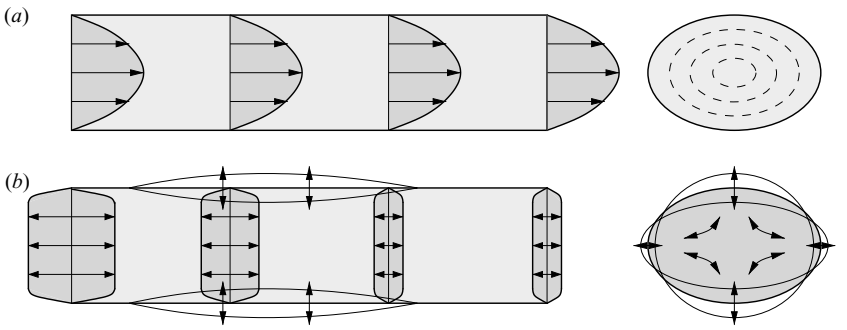

FIGURE 3. Sketches of the expected flow structure for an axially uniform elliptical tube with pressure boundary conditions. (*a*) The steady component of the axial velocity in a Poiseuille-like flow. (*b*) The oscillatory component with fundamental frequency. The oscillations in the axial velocity are expected to be larger in the rigid section that offers less inertial resistance (by being shorter, for example) to the oscillatory flow.

$|\hat{\boldsymbol{n}}^{\perp}| = 1$ and $\hat{\boldsymbol{n}}^{\perp} \cdot \hat{\boldsymbol{z}} = 0$). By substituting (2.32) into $\hat{\boldsymbol{n}} \cdot \hat{\boldsymbol{n}} = 1$, we find that

$$H_Z^{\mathrm{s}} = (1 - G^2\ell^{-2})^{-1/2} = 1 + O(\epsilon). \tag{2.33}$$

Since G is a measure of constriction or dilation of the tube cross-section as z increases, it also appears in the expression relating axial derivatives of quantities to those of their cross-sectional integrals. For an arbitrary scalar field $\psi(\check{\boldsymbol{r}})$, we obtain

$$\frac{\mathrm{d}}{\mathrm{d}\check{z}} \iint_{\mathscr{A}_0} \psi \, \mathrm{d}A = \iint_{\mathscr{A}_0} \frac{\partial \psi}{\partial \check{z}} \, \mathrm{d}A - \oint_{\mathscr{C}_0} \psi \, G H_Y^{\mathrm{s}} H_Z^{\mathrm{s}} \, \mathrm{d}\check{Y}, \tag{2.34}$$

by applying the divergence theorem to $\psi\hat{\boldsymbol{z}}$ over an infinitesimal volume of the tube between $\check{z}$ and $\check{z} + \mathrm{d}\check{z}$. This result will be used later in § 5.

3. Solution structure and rescaling

It is convenient to use several simultaneous decompositions to aid analytic progress. In particular, we decompose the variables and the equations into three components: a steady component, the oscillatory component with frequency $\check{\omega}$ and the remaining oscillatory components of higher frequency that arise from nonlinear interactions.

Since $\alpha \gg 1$ we expect the solution for the oscillatory motion to display a boundary-layer structure with inviscid flow away from the boundaries and viscous boundary layers of thickness $\alpha^{-1} = O(\epsilon)$ adjacent to the walls. We shall, therefore, consider the two regions separately and match the velocity and pressure fields between the two.

Finally, for each of the three components in the core and boundary-layer regions, we shall employ asymptotic expansions in the small parameters ϵ and δ.

A sketch of the expected form of the flow is shown in figure 3.

3.1. *Temporal decomposition and rescaling*

The non-dimensionalization described in § 2.4 was important to allow the structure of the equations to be seen, and motivate the scalings that followed in § 2.5. However, we can now see that there are two different velocity scales in the problem: that of the mean flow and that of the induced oscillatory flow. There are also several possible pressure scales, arising from balances between different terms in the equations. As a result, it is convenient to use different scales for the different components of each

variable. We, therefore, refine the previous non-dimensionalization and write the velocity and pressure as

$$\breve{\boldsymbol{u}} = \bar{\boldsymbol{u}} + \lambda\delta\tilde{\boldsymbol{u}} + \lambda\epsilon\delta^2\hat{\boldsymbol{u}}, \tag{3.1a}$$

$$\breve{p} = \frac{\epsilon}{\lambda}\bar{p} + \lambda\delta\tilde{p} + \lambda\epsilon\delta^2\hat{p}. \tag{3.1b}$$

The transverse and axial velocity components are similarly decomposed as

$$\breve{\boldsymbol{u}}^\perp = \bar{\boldsymbol{u}}^\perp + \lambda\delta\tilde{\boldsymbol{u}}^\perp + \lambda\epsilon\delta^2\hat{\boldsymbol{u}}^\perp, \tag{3.1c}$$

$$\breve{w} = \bar{w} + \lambda\delta\tilde{w} + \lambda\epsilon\delta^2\hat{w}. \tag{3.1d}$$

Overbars indicate the steady components, tildes the frequency-$\breve{\omega}$ components and carets the higher-frequency components. The various scales have been chosen so that the typical magnitude of each dimensionless variable is $O(1)$.

The steady axial velocity retains the previous scaling (based on the background flow). The steady pressure scale is amended to use the (smaller) nonlinear inertial scale $\epsilon/\lambda = 1/(\ell St)$; see (2.21*c*). The scale for the frequency-$\breve{\omega}$ velocity is amended by a factor of $\delta\lambda \equiv \Delta\ell St$ to match the velocities induced by the transverse wall motion. The corresponding pressure scale is adjusted in the same way, since the original unsteady inertial balance is expected to be dominant.

The scales for the higher-frequency components are chosen by balancing the unsteady inertia and axial pressure gradients with the nonlinear inertia from the interaction of the frequency-$\breve{\omega}$ velocity with itself; see (3.4).

We now substitute the expressions (3.1) into (2.21) and decompose the resulting equations into the same three components. We introduce the notation $[\![\,\cdot\,]\!]_n$ to denote the component with frequency $n\breve{\omega}$. The steady components are given by

$$\breve{\nabla}_\perp \cdot \bar{\boldsymbol{u}}^\perp + \frac{\partial \bar{w}}{\partial \breve{z}} = 0, \tag{3.2a}$$

$$(\bar{\boldsymbol{u}}\cdot\breve{\nabla})\bar{\boldsymbol{u}}^\perp + (\lambda\delta)^2[\![(\tilde{\boldsymbol{u}}\cdot\breve{\nabla})\tilde{\boldsymbol{u}}^\perp]\!]_0 + (\lambda\epsilon\delta^2)^2[\![(\hat{\boldsymbol{u}}\cdot\breve{\nabla})\hat{\boldsymbol{u}}^\perp]\!]_0 = -\frac{1}{\epsilon\beta}\breve{\nabla}_\perp\bar{p} + \frac{\lambda\epsilon}{R^2}\breve{\nabla}_\perp^2\bar{\boldsymbol{u}}^\perp + \frac{\lambda\beta\epsilon^2}{R^2}\frac{\partial^2\bar{\boldsymbol{u}}^\perp}{\partial\breve{z}^2}, \tag{3.2b}$$

$$(\bar{\boldsymbol{u}}\cdot\breve{\nabla})\bar{w} + (\lambda\delta)^2[\![(\tilde{\boldsymbol{u}}\cdot\breve{\nabla})\tilde{w}]\!]_0 + (\lambda\epsilon\delta^2)^2[\![(\hat{\boldsymbol{u}}\cdot\breve{\nabla})\hat{w}]\!]_0 = -\frac{\partial\bar{p}}{\partial\breve{z}} + \frac{\lambda\epsilon}{R^2}\breve{\nabla}_\perp^2\bar{w} + \frac{\lambda\beta\epsilon^2}{R^2}\frac{\partial^2\bar{w}}{\partial\breve{z}^2}. \tag{3.2c}$$

The frequency-$\breve{\omega}$ components are

$$\breve{\nabla}_\perp \cdot \tilde{\boldsymbol{u}}^\perp + \frac{\partial \tilde{w}}{\partial \breve{z}} = 0, \tag{3.3a}$$

$$\frac{\partial\tilde{\boldsymbol{u}}^\perp}{\partial\breve{t}} + \frac{\epsilon}{\lambda}\{(\bar{\boldsymbol{u}}\cdot\breve{\nabla})\tilde{\boldsymbol{u}}^\perp + (\tilde{\boldsymbol{u}}\cdot\breve{\nabla})\bar{\boldsymbol{u}}^\perp\} + \epsilon^2\delta^2[\![(\hat{\boldsymbol{u}}\cdot\breve{\nabla})\tilde{\boldsymbol{u}}^\perp + (\tilde{\boldsymbol{u}}\cdot\breve{\nabla})\hat{\boldsymbol{u}}^\perp]\!]_1 + \epsilon^3\delta^3[\![(\hat{\boldsymbol{u}}\cdot\breve{\nabla})\hat{\boldsymbol{u}}^\perp]\!]_1 = -\frac{1}{\epsilon\beta}\breve{\nabla}_\perp\tilde{p} + \frac{\epsilon^2}{R^2}\breve{\nabla}_\perp^2\tilde{\boldsymbol{u}}^\perp + \frac{\beta\epsilon^3}{R^2}\frac{\partial^2\tilde{\boldsymbol{u}}^\perp}{\partial\breve{z}^2}, \tag{3.3b}$$

$$\frac{\partial\tilde{w}}{\partial\breve{t}} + \frac{\epsilon}{\lambda}\{(\bar{\boldsymbol{u}}\cdot\breve{\nabla})\tilde{w} + (\tilde{\boldsymbol{u}}\cdot\breve{\nabla})\bar{w}\} + \epsilon^2\delta^2[\![(\hat{\boldsymbol{u}}\cdot\breve{\nabla})\tilde{w} + (\tilde{\boldsymbol{u}}\cdot\breve{\nabla})\hat{w}]\!]_1 + \epsilon^3\delta^3[\![(\hat{\boldsymbol{u}}\cdot\breve{\nabla})\hat{w}]\!]_1 = -\frac{\partial\tilde{p}}{\partial\breve{z}} + \frac{\epsilon^2}{R^2}\breve{\nabla}_\perp^2\tilde{w} + \frac{\beta\epsilon^3}{R^2}\frac{\partial^2\tilde{w}}{\partial\breve{z}^2}. \tag{3.3c}$$

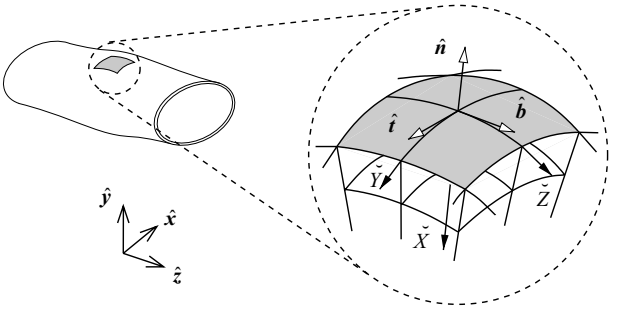

FIGURE 4. A sketch depicting the boundary-layer coordinate system showing the three unit vectors aligned with the (shaded) boundary surface in the steady configuration. Here $\hat{\boldsymbol{n}}$ is defined to be normal to the tube wall, while $\hat{\boldsymbol{t}}$ and $\hat{\boldsymbol{b}}$ lie in the surface.

The higher-frequency components are

$$\check{\nabla}_\perp \cdot \hat{\boldsymbol{u}}^\perp + \frac{\partial \hat{w}}{\partial \check{z}} = 0, \tag{3.4a}$$

$$\frac{\partial \hat{\boldsymbol{u}}^\perp}{\partial \check{t}} + \frac{\epsilon}{\lambda}\left\{(\bar{\boldsymbol{u}}\cdot\check{\nabla})\hat{\boldsymbol{u}}^\perp + (\hat{\boldsymbol{u}}\cdot\check{\nabla})\bar{\boldsymbol{u}}^\perp\right\} + \epsilon\delta[\![(\hat{\boldsymbol{u}}\cdot\check{\nabla})\tilde{\boldsymbol{u}}^\perp + (\tilde{\boldsymbol{u}}\cdot\check{\nabla})\hat{\boldsymbol{u}}^\perp]\!]_{2+}$$
$$+ [\![(\tilde{\boldsymbol{u}}\cdot\check{\nabla})\tilde{\boldsymbol{u}}^\perp]\!]_2 + \epsilon^2\delta^2[\![(\hat{\boldsymbol{u}}\cdot\check{\nabla})\hat{\boldsymbol{u}}^\perp]\!]_{2+} = -\frac{1}{\epsilon\beta}\check{\nabla}_\perp\hat{p} + \frac{\epsilon^2}{R^2}\check{\nabla}_\perp^2\hat{\boldsymbol{u}}^\perp + \frac{\beta\epsilon^3}{R^2}\frac{\partial^2\hat{\boldsymbol{u}}^\perp}{\partial\check{z}^2}, \tag{3.4b}$$

$$\frac{\partial \hat{w}}{\partial \check{t}} + \frac{\epsilon}{\lambda}\left\{(\bar{\boldsymbol{u}}\cdot\check{\nabla})\hat{w} + (\hat{\boldsymbol{u}}\cdot\check{\nabla})\bar{w}\right\} + \epsilon\delta[\![(\hat{\boldsymbol{u}}\cdot\check{\nabla})\tilde{w} + (\tilde{\boldsymbol{u}}\cdot\check{\nabla})\hat{w}]\!]_{2+}$$
$$+ [\![(\tilde{\boldsymbol{u}}\cdot\check{\nabla})\tilde{w}]\!]_2 + \epsilon^2\delta^2[\![(\hat{\boldsymbol{u}}\cdot\check{\nabla})\hat{w}]\!]_{2+} = -\frac{\partial\hat{p}}{\partial\check{z}} + \frac{\epsilon^2}{R^2}\check{\nabla}_\perp^2\hat{w} + \frac{\beta\epsilon^3}{R^2}\frac{\partial^2\hat{w}}{\partial\check{z}^2}. \tag{3.4c}$$

These sets of equations are exact and are equivalent to the original dimensionless governing equations (2.21).

Equations (3.2)–(3.4) also apply in the Stokes layer near the boundary, but there the shorter length scale in the direction normal to the wall promotes some of the viscous terms to leading order. The appropriate scalings and coordinates for the Stokes boundary layer are discussed in § 3.2. Discussion of the boundary conditions at the tube ends is deferred until § 3.3.

3.2. *Coordinates and equations for the Stokes layer*

We have assumed above that the $O(\epsilon\delta a)$ amplitude of the wall oscillations is smaller than the $O(\epsilon a)$ thickness of the boundary layer. Therefore, we are able to use stationary boundary-layer coordinates and linearize the boundary conditions onto the position of the tube wall in the steady configuration. A scaled normal coordinate $\check{X}$ in the $-\hat{\boldsymbol{n}}$ direction is added to the surface coordinates $(\check{Y}, \check{Z})$ to provide the coordinate system for the boundary layer (see figure 4). Full details of the coordinate system, together with the components of the equations and boundary conditions, can be found in Appendix A.

We decompose the velocity into the directions of the coordinate system, writing

$$\check{\boldsymbol{u}} = \check{\boldsymbol{U}} \equiv \check{U}\hat{\boldsymbol{n}} + \check{V}\hat{\boldsymbol{t}} + \ell\check{W}\hat{\boldsymbol{b}}. \tag{3.5}$$

The pressure and velocity components are decomposed into frequency components in a similar manner to (3.1). We write

$$\check{U} = \bar{U} + \lambda\delta\tilde{U} + \lambda\epsilon\delta^2\hat{U}, \tag{3.6a}$$

$$\check{V} = \bar{V} + \lambda\delta\tilde{V} + \lambda\delta^2\hat{V}, \tag{3.6b}$$

$$\check{W} = \bar{W} + \lambda\delta\tilde{W} + \lambda\delta^2\hat{W}, \tag{3.6c}$$

$$\check{P} = \frac{\epsilon}{\lambda}\bar{P} + \lambda\delta\tilde{P} + \lambda\epsilon\delta^2\hat{P}. \tag{3.6d}$$

Observe that the scales used for the tangential velocity components $\hat{V}$ and $\hat{W}$ are larger by a factor of ϵ than the corresponding scales (3.1) in the core. This is necessary in order to match the size of the largest contributions from the boundary conditions (A 13*b*) and (A 14*b*). As we shall see in § 7.2, the components with this larger scale can still be matched successfully with the flow in the core by insisting that they tend to zero as $\check{X} \to \infty$; this does not present any additional problems in the continuity equation.

To aid the expression of the matching conditions and composite expansions, we introduce notation for the asymptotic behaviour of the boundary-layer variables as $\check{X} \to \infty$. For the pressure, we write

$$\check{P} \sim \check{P}^{\infty} + \check{P}'^{\infty}\check{X} + \frac{1}{2}\check{P}''^{\infty}\check{X}^2 + \cdots, \tag{3.7}$$

where the superscript '∞' denotes the 'outer limit' of the velocity in the boundary layer as $\check{X} \to \infty$. Analogous expansions are used for the other variables.

3.3. *Boundary conditions at the tube ends*

The upstream pressure condition (2.11*a*) implies that

$$\check{p} = 0, \quad \check{P} = 0 \quad \text{at} \quad \check{z} = 0. \tag{3.8a,b}$$

If we impose a pressure condition at the downstream end, then (2.11*b*) implies

$$\check{p} = -\frac{\epsilon^2}{kR^2}, \quad \check{P} = -\frac{\epsilon^2}{kR^2} \quad \text{at} \quad \check{z} = 1. \tag{3.9a,b}$$

Alternatively, if we impose a flux condition (2.10) at $\check{z} = 1$, then we need to introduce a composite expansion $\check{w}_{comp}$ for the axial velocity. We have that

$$\check{w}_{comp} = \check{w} + \frac{1}{H_Z^s}(\check{W} - \check{W}^{\infty} - \check{X}\check{W}'^{\infty}) + \epsilon\beta G(\check{U} - \check{U}^{\infty}) + O(\epsilon^2), \tag{3.10}$$

allowing us to write (2.10) as

$$\iint_{\mathscr{A}_0(1)} \check{w}\,\mathrm{d}A + \epsilon \oint_{\mathscr{C}_0(1)} \left[\int_0^{\infty} (\check{W} - \check{W}^{\infty})\,\mathrm{d}\check{X}\right] H_Y^s\,\mathrm{d}\check{Y} + O(\epsilon^2) = \pi. \tag{3.11}$$

These boundary conditions are then decomposed into the different frequency components in the obvious way.

4. Solution for the steady flow (part I)

The solution of a steady high-Reynolds-number flow problem in anything but the simplest of tube geometries is far from straightforward (see Smith 1976*a*,*b*, for example). Fortunately, the exact details of the steady flow are unnecessary for evaluating the leading-order oscillatory flow and associated energy transfer. All the

information that is required is contained in the (non-dimensional) time-averaged volume flux

$$\mathcal{Q} = [\![\iint_{\mathscr{A}} \breve{w}_{comp} \, \mathrm{d}A]\!]_0, \tag{4.1}$$

where $\breve{w}_{comp}$ is given by (3.10). For the pressure–flux case, $\mathcal{Q} = \pi$ is fixed by the downstream boundary condition (2.10). For the pressure–pressure case, $\mathcal{Q}$ is derived from the solution to the steady flow problem, which may require numerical computation.

4.1. *Series expansion for the steady flow*

The equations and boundary conditions for the steady problem suggest using a double series expansion in powers of ϵ and δ. However, at this stage it is sufficient to expand only in δ. (Each term in this expansion then implicitly includes all powers of ϵ.) We also note that symmetry considerations (specifically the invariance of the full problem under $\delta \mapsto -\delta$, $\breve{t} \mapsto \breve{t} + \pi/\breve{\omega}$) mean that only even powers of δ are present in the steady problem. We therefore write

$$\bar{\boldsymbol{u}} = \bar{\boldsymbol{u}}_0 + \delta^2 \bar{\boldsymbol{u}}_2 + O(\delta^4), \tag{4.2a}$$

$$\bar{p} = \bar{p}_0 + \delta^2 \bar{p}_2 + O(\delta^4). \tag{4.2b}$$

The boundary-layer structure for the steady flow is potentially quite complicated and certainly depends on the entrance flow profile at the upstream end. For fully developed flow in a uniform tube, there will be no boundary layer at leading order. For a plug-flow injection, there will be a viscous layer that grows as $\breve{z}$ increases downstream. In addition, products of oscillatory terms will contribute at higher orders and result in a forcing of the equations that has a boundary-layer structure. At leading order, we shall just consider the domain as a single region and not make any decomposition into boundary layers.

4.2. *Steady flow at* $O(\delta^0)$

From (3.2), the leading-order equations for the steady flow are

$$\breve{\nabla}_\perp \cdot \bar{\boldsymbol{u}}_0^\perp + \frac{\partial \bar{w}_0}{\partial \breve{z}} = 0, \tag{4.3a}$$

$$(\bar{\boldsymbol{u}}_0 \cdot \breve{\nabla}) \bar{\boldsymbol{u}}_0^\perp = -\frac{1}{\epsilon\beta} \breve{\nabla}_\perp \bar{p}_0 + \frac{\lambda\epsilon}{R^2} \breve{\nabla}_\perp^2 \bar{\boldsymbol{u}}_0^\perp + \frac{\lambda\beta\epsilon^2}{R^2} \frac{\partial^2 \bar{\boldsymbol{u}}_0^\perp}{\partial \breve{z}^2}, \tag{4.3b}$$

$$(\bar{\boldsymbol{u}}_0 \cdot \breve{\nabla}) \bar{w}_0 = -\frac{\partial \bar{p}_0}{\partial \breve{z}} + \frac{\lambda\epsilon}{R^2} \breve{\nabla}_\perp^2 \bar{w}_0 + \frac{\lambda\beta\epsilon^2}{R^2} \frac{\partial^2 \bar{w}_0}{\partial \breve{z}^2}. \tag{4.3c}$$

These are simply the steady Navier–Stokes equations, written in a dimensionless form. The boundary conditions are

$$\bar{\boldsymbol{u}}_0 = \boldsymbol{0} \quad \text{on} \quad \mathscr{W}_0, \tag{4.4}$$

and the appropriate conditions at the tube ends. For the flux–pressure case, we have

$$\bar{p}_0 = 0 \quad \text{at} \quad \breve{z} = 0, \qquad \iint_{\mathscr{A}_0} \bar{w}_0 \, \mathrm{d}A = \pi \quad \text{at} \quad \breve{z} = 1. \tag{4.5a,b}$$

For the pressure–pressure case, we have

$$\bar{p}_0 = 0 \quad \text{at} \quad \breve{z} = 0, \qquad \bar{p}_0 = -\frac{\epsilon\lambda}{kR^2} \quad \text{at} \quad \breve{z} = 1. \tag{4.6a,b}$$

At this order, the mean flux is given by

$$\mathcal{Q}_0 = \iint_{\mathscr{A}_0} \bar{w}_0 \, \mathrm{d}A. \tag{4.7}$$

The system represents the flow through the tube in the steady configuration, i.e. in the absence of oscillations. As stated, the problem is not fully specified, since there is the freedom to choose a flow profile at the inlet. However, to the orders that we are working, it is only the mean axial flux (rather than the details of the flow distribution) that is important.

4.3. *Steady flow at higher orders in* δ

The equations governing the steady flow at higher orders in δ involve oscillatory components, which we have yet to evaluate. Therefore, discussion thereof will be postponed until § 7.

However, we observe that, with pressure–pressure boundary conditions, there is a possibility that the largest component of $\bar{w}_2$ may be $O(\epsilon^{-1})$, resulting in an $O(\delta^2/\epsilon)$ axial velocity. If $\delta^2/\epsilon \gtrsim O(1)$, then this additional flow will be present at leading order, and so contributes to the leading-order volume flux. However, in § 2.5, we made the restriction $\delta^2 \leqslant \epsilon$, so we only need to consider this additional contribution for $\delta^2/\epsilon = O(1)$.

The $O(\delta^2/\epsilon)$ axial velocity can arise as follows. If the dominant resistance to the axial flow is viscous, then (4.3*c*) shows that an $O(\epsilon)$ pressure gradient will drive an $O(1)$ axial velocity. Consequently, the addition of an $O(\delta^2)$ forcing term as present in (3.2*c*) could potentially induce an $O(\delta^2/\epsilon)$ axial flow. In the case of pressure–pressure boundary conditions, we find that this mechanism does indeed lead to a change in axial velocity of $O(\delta^2/\epsilon)$ (hence the earlier restriction $\delta^2 \lesssim \epsilon$). For pressure–flux boundary conditions, the extra forcing can be absorbed by a modified pressure at leading order, and there is no change in the leading-order axial velocity.

For use in the following sections, we therefore introduce the notation $\bar{\boldsymbol{u}}_{\oint}$, $\bar{p}_{\oint}$, $\mathcal{Q}_{\oint}$ to represent the true $O(1)$ components of the steady velocity, pressure and flux; i.e. including all the terms proportional to $\epsilon^n\delta^m$ where $\epsilon^n\delta^m = O(1)$. In the natural way, we define

$$\mathcal{Q}_{\oint} = \iint_{\mathscr{A}_0} \bar{w}_{\oint}\,\mathrm{d}A \tag{4.8}$$

as the leading-order steady flux.

5. The fundamental oscillatory flow

The motion of the boundary drives an oscillatory flow in the core. Changes in the cross-sectional area force an axial sloshing flow $\tilde{w}$, and changes in the boundary shape result in an additional flow $\tilde{\boldsymbol{u}}^{\perp}$ within each cross-section.

We expand the oscillatory velocity in a double power series in ϵ and δ. However, symmetry considerations, and the fact that δ enters only through an $\epsilon\delta$ combination, mean that several of the coefficients (particularly lower combinations containing δ) are zero. Taking into account these simplifications, the first few terms in the expansion in the core are

$$\tilde{\boldsymbol{u}} = \mathrm{Re}\big[\mathrm{e}^{\mathrm{i}\check{\omega}\check{t}}\big(\tilde{\boldsymbol{u}}_{00} + \epsilon\tilde{\boldsymbol{u}}_{01} + \epsilon^2\tilde{\boldsymbol{u}}_{02} + O(\epsilon^3, \epsilon^2\delta^2)\big)\big], \tag{5.1a}$$

$$\tilde{p} = \mathrm{Re}\big[\mathrm{e}^{\mathrm{i}\check{\omega}\check{t}}\big(\tilde{p}_{00} + \epsilon\tilde{p}_{01} + \epsilon^2\tilde{p}_{02} + O(\epsilon^3, \epsilon^2\delta^2)\big)\big], \tag{5.1b}$$

where $\tilde{\boldsymbol{u}}_{00}$, $\tilde{\boldsymbol{u}}_{01}$ etc. are complex-valued functions of position, and the two subscripts denote the powers of δ and ϵ, respectively. Similarly, in the Stokes layer, we write

$$\tilde{\boldsymbol{U}} = \mathrm{Re}\big[\mathrm{e}^{\mathrm{i}\check{\omega}\check{t}}\big(\tilde{\boldsymbol{U}}_{00} + \epsilon\tilde{\boldsymbol{U}}_{01} + \epsilon^2\tilde{\boldsymbol{U}}_{02} + O(\epsilon^3, \epsilon^2\delta^2)\big)\big], \tag{5.2a}$$

$$\tilde{P} = \mathrm{Re}\big[\mathrm{e}^{\mathrm{i}\check{\omega}\check{t}}\big(\tilde{P}_{00} + \epsilon\tilde{P}_{01} + \epsilon^2\tilde{P}_{02} + O(\epsilon^3, \epsilon^2\delta^2)\big)\big]. \tag{5.2b}$$

These expressions are substituted into (3.3) and their analogues from (A 6) and (A 7), respectively.

5.1. *The oscillatory core flow at* $O(\epsilon^{-1})$

Only one term in (3.3) is present at this order and hence must vanish. We have

$$\check{\nabla}_\perp \tilde{p}_{00} = \mathbf{0}, \tag{5.3}$$

so the leading-order pressure is uniform in each cross-section. The details of the flow field and axial pressure variations enter only at the next order in ϵ.

5.2. *The oscillatory flow in the Stokes layer at* $O(\epsilon^{-1})$

Only two of the governing equations (A 6) and (A 7) have terms at this order. In both cases, it is a single term, which must therefore vanish. We have

$$\frac{\partial \tilde{U}_{00}}{\partial \check{X}} = 0, \quad \frac{\partial \tilde{P}_{00}}{\partial \check{X}} = 0. \tag{5.4a,b}$$

Hence, the leading-order normal velocity and pressure at the boundary are transmitted unchanged through the thin Stokes layer to the core flow. From (A 12*b*) and (A 15*a*), the relevant boundary and matching conditions are

$$\tilde{U}_{00}(0, \check{Y}, \check{Z}) = \mathrm{i}\check{\omega}\,\xi(\check{Y}, \check{Z}), \quad \tilde{P}^{\infty}_{00}(\check{Y}, \check{Z}) = \tilde{p}_{00}|_{\mathscr{C}_0}, \tag{5.5a,b}$$

and hence

$$\tilde{U}_{00} = \mathrm{i}\check{\omega}\,\xi(\check{Y}, \check{Z}), \quad \tilde{P}_{00} = \tilde{p}_{00}(\check{Z}), \tag{5.6a,b}$$

throughout the Stokes boundary layer.

5.3. *The oscillatory core flow at* $O(1)$

The relevant components of (3.3) are

$$\check{\nabla}_\perp \cdot \tilde{\boldsymbol{u}}^{\perp}_{00} + \frac{\partial \tilde{w}_{00}}{\partial \check{z}} = 0, \tag{5.7a}$$

$$\check{\nabla}_\perp \tilde{p}_{01} = -\mathrm{i}\check{\omega}\beta\tilde{\boldsymbol{u}}^{\perp}_{00}, \tag{5.7b}$$

$$\frac{\partial \tilde{p}_{00}}{\partial \check{z}} = -\mathrm{i}\check{\omega}\tilde{w}_{00}. \tag{5.7c}$$

Matching with the Stokes layer at the wall, we have from (A 15*b*)

$$\hat{\boldsymbol{n}} \cdot \left(\tilde{\boldsymbol{u}}^{\perp}_{00} + \ell\tilde{w}_{00}\hat{\boldsymbol{z}}\right) = \tilde{U}^{\infty}_{00} \quad \text{on} \quad \mathscr{W}_0, \tag{5.8a}$$

which, using (2.32) and (5.6*a*), implies

$$H_Z^{\mathrm{s}\,-1}\hat{\boldsymbol{n}}^{\perp} \cdot \tilde{\boldsymbol{u}}^{\perp}_{00} + G\tilde{w}_{00} = \mathrm{i}\check{\omega}\,\xi \quad \text{on} \quad \mathscr{W}_0. \tag{5.8b}$$

The pressure condition (3.8*a*) at the upstream end implies

$$\tilde{p}_{00}(0) = 0. \tag{5.8c}$$

At the downstream end, we have either

$$\iint_{\mathscr{A}_0(1)} \tilde{w}_{00}\,\mathrm{d}A = 0 \quad \text{or} \quad \tilde{p}_{00}(1) = 0, \tag{5.8d,e}$$

from (3.11) or (3.9*a*), respectively, for a flux or pressure condition.

We now use the result (2.34) with $\psi = \tilde{w}_{00}$. Substituting from (5.7*a*) and applying the divergence theorem in the cross-section, we obtain

$$\frac{\mathrm{d}}{\mathrm{d}\check{z}} \iint_{\mathscr{A}_0} \tilde{w}_{00}\,\mathrm{d}A = -\oint_{\mathscr{C}_0} \left(\tilde{\boldsymbol{u}}_{00}^{\perp} \cdot \hat{\boldsymbol{n}}^{\perp} + G H_Z^{\mathrm{s}} \tilde{w}_{00}\right) H_Y^{\mathrm{s}}\,\mathrm{d}\check{Y}. \tag{5.9}$$

Using the boundary condition (5.8*b*) and the fact that $\check{\nabla}_{\perp}\tilde{w}_{00} = \boldsymbol{0}$ from (5.3) and (5.7*c*), we obtain

$$\frac{\mathrm{d}}{\mathrm{d}\check{z}}(\tilde{w}_{00}(\check{z})\,A_0(\check{z})) = -\mathrm{i}\check{\omega}\tilde{A}(\check{z}), \tag{5.10}$$

where

$$\tilde{A}(\check{z}) = \oint_{\mathscr{C}_0(\check{z})} \xi\, H_Y^{\mathrm{s}} H_Z^{\mathrm{s}}\,\mathrm{d}Y \tag{5.11}$$

is the effective oscillatory area change in each cross-section, and A_0 is the cross-sectional area of the tube in the steady configuration. Applying the pressure boundary condition (5.8*c*) at $\check{z} = 0$, we can integrate (5.7*c*) to obtain

$$\tilde{p}_{00}(\check{z}) = -\mathrm{i}\check{\omega}\int_0^{\check{z}} \tilde{w}_{00}(\check{z}')\,\mathrm{d}\check{z}'. \tag{5.12}$$

It is convenient to introduce an effective volume variation $\tilde{\mathbb{V}}(\check{z})$ by expressing the axial velocity and pressure as

$$\tilde{w}_{00}(\check{z}) = -\frac{\mathrm{i}\check{\omega}\tilde{\mathbb{V}}(\check{z})}{A_0(\check{z})}, \quad \tilde{p}_{00}(\check{z}) = -\check{\omega}^2 \int_0^{\check{z}} \frac{\tilde{\mathbb{V}}(\check{z}')}{A_0(\check{z}')}\,\mathrm{d}\check{z}'. \tag{5.13a,b}$$

The equation for $\tilde{\mathbb{V}}$ is then

$$\frac{\mathrm{d}\tilde{\mathbb{V}}}{\mathrm{d}\check{z}} = \tilde{A} \tag{5.14}$$

subject to either

$$\tilde{\mathbb{V}}(1) = 0 \quad \text{or} \quad \int_0^1 \frac{\tilde{\mathbb{V}}(\check{z})}{A_0(\check{z})}\,\mathrm{d}\check{z} = 0, \tag{5.15a,b}$$

for pressure–flux or pressure–pressure end conditions respectively. We adopt a Green's-function representation for the solution of (5.14), writing

$$\tilde{\mathbb{V}}(\check{z}) = \int_0^{\check{z}} \chi(\check{z}')\tilde{A}(\check{z}')\,\mathrm{d}\check{z}' - \int_{\check{z}}^1 (1-\chi(\check{z}'))\tilde{A}(\check{z}')\,\mathrm{d}\check{z}', \tag{5.16}$$

where χ is independent of $\tilde{A}$. For the case of the flux condition, applying (5.15*a*) to (5.16) we obtain

$$\chi(\check{z}) \equiv 0. \tag{5.17}$$

For the pressure condition, by substituting (5.16) into (5.15*b*) and exchanging the order of integration, we find that

$$\chi(\check{z}) = \int_0^{\check{z}} \frac{1}{A_0(\check{z}')}\,\mathrm{d}\check{z}' \Bigg/ \int_0^1 \frac{1}{A_0(\check{z}')}\,\mathrm{d}\check{z}'\,. \tag{5.18}$$

Physically, $\chi(\check{z})$ is the proportion of the additional oscillatory flow generated by the area changes $\tilde{A}(\check{z})$ at $\check{z}$ that goes downstream from $\check{z}$. With a flux condition at $\check{z} = 1$, all the flow must go upstream, and hence $\chi = 0$. With a pressure condition at both

ends, the flow partitions in inverse proportion to the inertance (inertial resistance to oscillatory flow) in the upstream and downstream segments.

We now examine the problem for the cross-sectional flow. Combining (5.7*a*), (5.7*b*) and (5.8*b*), we arrive at a Poisson problem for $\tilde{p}_{01}$, which can be solved independently in each cross-section:

$$\check{\nabla}_{\perp}^2 \tilde{p}_{01} = \mathrm{i}\check{\omega}\beta \frac{\partial \tilde{w}_{00}}{\partial \check{z}} \quad \text{in } \mathscr{A}_0, \tag{5.19a}$$

$$\hat{\boldsymbol{n}}^{\perp} \cdot \check{\nabla}_{\perp} \tilde{p}_{01} = \beta H_Z^{\mathrm{s}} (\check{\omega}^2 \xi + \mathrm{i}\check{\omega} G \tilde{w}_{00}) \quad \text{on } \mathscr{C}_0. \tag{5.19b}$$

Since we have Neumann boundary conditions, $\tilde{p}_{01}$ is only defined at this stage up to an arbitrary function of $\check{z}$. We therefore define the cross-sectionally averaged component

$$\tilde{p}_{01}^{*}(\check{z}) \equiv \frac{1}{A_0(\check{z})} \iint_{\mathscr{A}_0} \tilde{p}_{01} \, \mathrm{d}A, \tag{5.20}$$

and write

$$\tilde{p}_{01} = \tilde{p}_{01}^{*}(\check{z}) + \tilde{p}_{01}^{\triangle}(\check{x}, \check{y}, \check{z}). \tag{5.21}$$

Therefore, $\tilde{p}_{01}^{\triangle}$ is the solution of (5.19) that also satisfies

$$\iint_{\mathscr{A}_0} \tilde{p}_{01}^{\triangle} \, \mathrm{d}A = 0. \tag{5.22}$$

The pressure component $\tilde{p}_{01}^{\triangle}$ is now well defined and can be computed explicitly. It can be used to recover the cross-sectional flow $\tilde{\boldsymbol{u}}_{00}^{\perp}$ from (5.7*b*) since $\nabla_{\perp} \tilde{p}_{01}^{\triangle} = \nabla_{\perp} \tilde{p}_{01}$. The axial variation of $\tilde{p}_{01}$, and hence $\tilde{p}_{01}^{*}$, is governed by the core equations at $O(\epsilon)$, subject to conditions at the tube ends. The solution is presented in § 5.5.

5.4. *The oscillatory flow in the Stokes layer at* $O(1)$

As the tube wall is approached, the tangential components of the $O(1)$ flow in the core (e.g. (5.13*a*)) will not, in general, match the tangential velocity of the wall. At this order viscous effects passively smooth the tangential velocities across the thickness of the Stokes layer. Since the displacements and boundary-layer thickness are both small, effects from the curvature and motion of the boundary are not present here.

Taking the appropriate components from (A 6) and (A 7), we find that the equations are

$$-\frac{\partial \tilde{U}_{01}}{\partial \check{X}} + \frac{\check{K}_Y}{H_Y^{\mathrm{s}}} \tilde{U}_{00} + \frac{1}{H_Y^{\mathrm{s}} H_Z^{\mathrm{s}}} \frac{\partial}{\partial \check{Y}} \left(H_Z^{\mathrm{s}} \tilde{V}_{00} \right) + \frac{1}{H_Y^{\mathrm{s}} H_Z^{\mathrm{s}}} \frac{\partial}{\partial \check{Z}} \left(H_Y^{\mathrm{s}} \tilde{W}_{00} \right) = 0, \tag{5.23a}$$

$$\frac{\partial \tilde{P}_{01}}{\partial \check{X}} = 0, \tag{5.23b}$$

$$\mathrm{i}\check{\omega} \tilde{V}_{00} = -\frac{1}{\beta H_Y^{\mathrm{s}}} \frac{\partial \tilde{P}_{01}}{\partial \check{Y}} + \frac{1}{R^2} \frac{\partial^2 \tilde{V}_{00}}{\partial \check{X}^2}, \tag{5.23c}$$

$$\mathrm{i}\check{\omega} \tilde{W}_{00} = -\frac{\partial \tilde{P}_{00}}{\partial \check{Z}} + \frac{1}{R^2} \frac{\partial^2 \tilde{W}_{00}}{\partial \check{X}^2}, \tag{5.23d}$$

with boundary conditions

$$\tilde{U}_{01} = 0, \quad \tilde{V}_{00} = \mathrm{i}\check{\omega}\, \eta, \quad \tilde{W}_{00} = 0 \quad \text{on} \quad \check{X} = 0, \tag{5.24a–c}$$

and matching conditions

$$\tilde{P}_{01} \to \tilde{P}_{01}^{\infty} = \tilde{p}_{01}|_{\mathscr{C}_0}, \quad \tilde{V}_{00} \to \tilde{V}_{00}^{\infty} = \hat{\boldsymbol{t}} \cdot \tilde{\boldsymbol{u}}_{00}^{\perp}|_{\mathscr{C}_0}, \quad \tilde{W}_{00} \to \tilde{W}_{00}^{\infty} = \tilde{w}_{00}|_{\mathscr{C}_0}, \tag{5.25a–c}$$

$$\frac{\partial \tilde{U}_{01}}{\partial X} \to \tilde{U}_{01}^{\prime\infty} = \hat{\boldsymbol{n}} \cdot \frac{\partial \tilde{\boldsymbol{u}}_{00}^{\perp}}{\partial n}\bigg|_{\mathscr{C}_0} + G\frac{\partial \tilde{w}_{00}}{\partial n}\bigg|_{\mathscr{C}_0} \quad \text{as} \quad \check{X} \to \infty, \tag{5.25d}$$

where $\partial/\partial n \equiv \hat{\boldsymbol{n}} \cdot \check{\boldsymbol{\nabla}}$.

There are no specific conditions to be satisfied at the tube ends at this order. The pressure already matches that in the core to satisfy (3.8*a*) and (3.9*a*), and the $O(\epsilon)$ component of the mass flux condition (3.11) also has contributions from the $O(\epsilon)$ core flow, which we have yet to determine.

Equation (5.23*c*) implies that $\tilde{P}_{01}$ is uniform across the Stokes layer, and hence is prescribed by the value in the core via (5.25*a*). Using (5.7*b*) and (5.7*c*), we can now express the derivatives of $\tilde{P}$ that appear in (5.23*c*) and (5.23*d*) in terms of the fluid velocity in the core. We have

$$\frac{\partial \tilde{P}_{01}}{\partial Y} = H_Y^{\mathrm{s}}\ \hat{\boldsymbol{t}} \cdot \check{\boldsymbol{\nabla}}_{\perp} \tilde{p}_{01}\Big|_{\mathscr{C}_0} = -\mathrm{i}\check{\omega}\beta\, H_Y^{\mathrm{s}}\ \hat{\boldsymbol{t}} \cdot \tilde{\boldsymbol{u}}_{00}^{\perp}\big|_{\mathscr{C}_0}, \tag{5.26a}$$

$$\frac{\partial \tilde{P}_{00}}{\partial \check{Z}} = \frac{\partial \tilde{p}_{00}}{\partial \check{z}}\bigg|_{\mathscr{C}_0} = -\mathrm{i}\check{\omega}\ \tilde{w}_{00}|_{\mathscr{C}_0}. \tag{5.26b}$$

The solution to (5.23)–(5.25) for $\tilde{V}_{00}$ and $\tilde{W}_{00}$ is then given by

$$\tilde{V}_{00} = \hat{\boldsymbol{t}} \cdot \tilde{\boldsymbol{u}}_{00}^{\perp}\big|_{\mathscr{C}_0}(1 - E(\check{X})) + \mathrm{i}\check{\omega}\,\eta\, E(\check{X}), \tag{5.27a}$$

$$\tilde{W}_{00} = \tilde{w}_{00}|_{\mathscr{C}_0}(1 - E(\check{X})), \tag{5.27b}$$

where we have introduced

$$E(\check{X}) \equiv \exp\left(-\left(\tfrac{1}{2}\check{\omega}\right)^{1/2}(1+\mathrm{i})\,R\check{X}\right). \tag{5.28}$$

Having found the two tangential components of the velocity, conservation of mass allows the correction to the normal velocity to be calculated. Integrating (5.23*b*) and applying the boundary condition (5.24*a*), we obtain

$$\begin{aligned}\tilde{U}_{01} = {} & \frac{(1-\mathrm{i})}{(2\check{\omega})^{1/2}R}\,\frac{1}{H_Y^{\mathrm{s}}H_Z^{\mathrm{s}}}\left[\frac{\partial}{\partial Y}\left(H_Z^{\mathrm{s}}\left(\mathrm{i}\check{\omega}\eta - \hat{\boldsymbol{t}} \cdot \tilde{\boldsymbol{u}}_{00}^{\perp}\big|_{\mathscr{C}_0}\right)\right) - \frac{\partial}{\partial \check{Z}}\left(H_Y^{\mathrm{s}}\tilde{w}_{00}\right)\right](1 - E(\check{X})) \\ & + \frac{1}{H_Y^{\mathrm{s}}H_Z^{\mathrm{s}}}\left[\frac{\partial}{\partial Y}\left(H_Z^{\mathrm{s}}\,\hat{\boldsymbol{t}} \cdot \tilde{\boldsymbol{u}}_{00}^{\perp}\big|_{\mathscr{C}_0}\right) + \frac{\partial}{\partial \check{Z}}\left(H_Y^{\mathrm{s}}\tilde{w}_{00}\right) + \mathrm{i}\check{\omega}H_Z^{\mathrm{s}}\check{K}_Y\xi\right]\check{X}.\end{aligned} \tag{5.29}$$

By applying incompressibility in the core (5.7*a*), it can be seen that this satisfies the final matching condition (5.25*d*). Comparing (5.29) with the expression $\tilde{U}_{01} \sim \tilde{U}_{01}^{\infty} + \tilde{U}_{01}^{\prime\infty}\check{X}$ as $\check{X} \to \infty$, we find that

$$\tilde{U}_{01}^{\infty} = \frac{(1-\mathrm{i})}{(2\check{\omega})^{1/2}R}\,\frac{1}{H_Y^{\mathrm{s}}H_Z^{\mathrm{s}}}\left[\frac{\partial}{\partial Y}\left(H_Z^{\mathrm{s}}\left(\mathrm{i}\check{\omega}\eta - \hat{\boldsymbol{t}} \cdot \tilde{\boldsymbol{u}}_{00}^{\perp}\big|_{\mathscr{C}_0}\right)\right) - \frac{\partial}{\partial \check{Z}}\left(H_Y^{\mathrm{s}}\tilde{w}_{00}\right)\right]. \tag{5.30}$$

This limiting value is used in the following section for matching with the core flow at $O(\epsilon)$.

5.5. *The oscillatory core flow at* $O(\epsilon)$

The oscillatory flow in the core at this order is forced from the walls by the normal velocity correction $\tilde{U}_{01}$ in the Stokes layer, and also in the interior by Reynolds stresses resulting from the interaction between the steady and oscillatory core flows

at $O(1)$. The relevant components of the governing equations (3.3) are

$$\check{\nabla}_\perp \cdot \tilde{\boldsymbol{u}}_{01}^\perp + \frac{\partial \tilde{w}_{01}}{\partial \check{z}} = 0, \tag{5.31a}$$

$$\mathrm{i}\check{\omega}\beta\, \tilde{\boldsymbol{u}}_{01}^\perp + \frac{\beta}{\lambda}\left[(\bar{\boldsymbol{u}}_\phi \cdot \check{\nabla})\tilde{\boldsymbol{u}}_{00}^\perp + (\tilde{\boldsymbol{u}}_{00} \cdot \check{\nabla})\bar{\boldsymbol{u}}_\phi^\perp\right] = -\check{\nabla}_\perp \tilde{p}_{02}, \tag{5.31b}$$

$$\mathrm{i}\check{\omega}\, \tilde{w}_{01} + \frac{1}{\lambda}\left[(\bar{\boldsymbol{u}}_\phi \cdot \check{\nabla})\tilde{w}_{00} + (\tilde{\boldsymbol{u}}_{00} \cdot \check{\nabla})\bar{w}_\phi\right] = -\frac{\partial \tilde{p}_{01}}{\partial \check{z}}, \tag{5.31c}$$

recalling that $\bar{\boldsymbol{u}}_\phi = \bar{\boldsymbol{u}}_\phi^\perp + \ell \bar{w}_\phi \hat{\boldsymbol{z}}$ is the leading-order steady velocity that was introduced in § 4.3. The boundary conditions are

$$H_Z^{\mathrm{s}\,-1}\hat{\boldsymbol{n}}^\perp \cdot \tilde{\boldsymbol{u}}_{01}^\perp + G\tilde{w}_{01} = \tilde{U}_{01}^\infty \quad \text{on} \quad \mathscr{C}_0, \tag{5.32a}$$

from the matching of the normal velocity to that in the Stokes layer, together with

$$\tilde{p}_{01} = 0 \quad \text{at} \quad \check{z} = 0, \tag{5.32b}$$

from the upstream pressure condition (3.8a), and either

$$\iint_{\mathscr{A}_0} \tilde{w}_{01}\, \mathrm{d}A = 0 \quad \text{or} \quad \tilde{p}_{01} = 0 \quad \text{at} \quad \check{z} = 1, \tag{5.32c,d}$$

from (3.9a) or (3.11) at the downstream end.

These equations are similar to their $O(1)$ counterparts (5.7), except for the additional Reynolds-stress terms. The method of solution is similar but slightly more involved since $\tilde{w}_{01}$ (unlike $\tilde{w}_{00}$) is not uniform in each cross-section. However, we must first complete the solution for $\tilde{p}_{01}$ by finding its cross-sectional average $\tilde{p}_{01}^*$ (see (5.20)), from which we can determine $\tilde{w}_{01}$ via (5.31c). Finally, we will formulate a Poisson problem for $\tilde{p}_{02}$, the solution of which allows the transverse velocity $\tilde{\boldsymbol{u}}_{01}^\perp$ to be found.

To determine $\tilde{p}_{01}^*$, we begin by noting that the Reynolds-stress terms in (5.31c) can be written as

$$S_R \equiv \tilde{\boldsymbol{u}}_{00} \cdot \check{\nabla}\bar{w}_\phi + \bar{\boldsymbol{u}}_\phi \cdot \check{\nabla}\tilde{w}_{00} = \check{\nabla}_\perp \cdot \left[\tilde{\boldsymbol{u}}_{00}^\perp \bar{w}_\phi + \bar{\boldsymbol{u}}_\phi^\perp \tilde{w}_{00}\right] + 2\frac{\partial}{\partial \check{z}}(\tilde{w}_{00}\bar{w}_\phi), \tag{5.33}$$

and hence

$$\iint_{\mathscr{A}_0} S_R\, \mathrm{d}A = \oint_{\mathscr{C}_0} \hat{\boldsymbol{n}}^\perp \cdot \left[\tilde{\boldsymbol{u}}_{00}^\perp \bar{w}_\phi + \bar{\boldsymbol{u}}_\phi^\perp \tilde{w}_{00}\right] H_Y^{\mathrm{s}}\, \mathrm{d}Y + 2\frac{\mathrm{d}}{\mathrm{d}\check{z}}\left(\tilde{w}_{00}\iint_{\mathscr{A}_0} \bar{w}_\phi\, \mathrm{d}A\right). \tag{5.34}$$

The first integral on the right-hand side of (5.34) vanishes, since $\hat{\boldsymbol{n}}^\perp \cdot \bar{\boldsymbol{u}}_\phi^\perp = \bar{w}_\phi = 0$ on $\mathscr{C}_0$ from (4.4). The same result allows us to move the derivative through the second integral despite the variations in $\mathscr{A}_0$ with $\check{z}$. Applying (4.8) we then obtain

$$\iint_{\mathscr{A}_0} S_R\, \mathrm{d}A = 2\mathcal{Q}_\phi \frac{\mathrm{d}\tilde{w}_{00}}{\mathrm{d}\check{z}}. \tag{5.35}$$

We now apply the result (2.34) with $\psi = \tilde{w}_{01}$, substituting from (5.31b) and (5.32a), to obtain

$$\frac{\mathrm{d}}{\mathrm{d}\check{z}}\iint_{\mathscr{A}_0} \tilde{w}_{01}\, \mathrm{d}A + \oint_{\mathscr{C}_0} \tilde{U}_{01}^\infty H_Y^{\mathrm{s}} H_Z^{\mathrm{s}}\, \mathrm{d}\check{Y} = 0. \tag{5.36}$$

Next, we integrate (5.31c) over each cross-section. Taking the derivative with respect to $\check{z}$, and using the results (5.35) and (5.36) and the decomposition (5.21), we obtain

$$\frac{\mathrm{d}}{\mathrm{d}\check{z}}\left(A_0(\check{z})\frac{\mathrm{d}\tilde{p}_{01}^*}{\mathrm{d}\check{z}}\right) = \mathrm{i}\check{\omega}\oint_{\mathscr{C}_0} \tilde{U}_{01}^\infty H_Y^{\mathrm{s}} H_Z^{\mathrm{s}}\, \mathrm{d}\check{Y} - \frac{2\mathcal{Q}_\phi}{\lambda}\frac{\mathrm{d}^2\tilde{w}_{00}}{\mathrm{d}\check{z}^2} - \frac{\mathrm{d}}{\mathrm{d}\check{z}}\iint_{\mathscr{A}_0} \frac{\partial \tilde{p}_{01}^\triangle}{\partial \check{z}}\, \mathrm{d}A. \tag{5.37}$$

This is a second-order ordinary differential equation for $\tilde{p}^*_{01}(\check{z})$ in terms of known quantities. Applying the pressure and flux conditions at the tube ends ties down the two constants of integration, and hence we can obtain $\tilde{p}^*_{01}(\check{z})$. With $\tilde{p}_{01}$ known, (5.31*c*) gives $\tilde{w}_{01}$.

We now turn to the transverse velocity $\tilde{\boldsymbol{u}}^{\perp}_{01}$. Eliminating $\tilde{\boldsymbol{u}}^{\perp}_{01}$ and $\tilde{w}_{01}$ between (5.31) results in the Poisson problem

$$\check{\nabla}^2_{\perp}\tilde{p}_{02} = -\frac{\beta}{\lambda}\nabla\cdot\left[(\bar{\boldsymbol{u}}_{\phi}\cdot\check{\nabla})\tilde{\boldsymbol{u}}_{00} + (\tilde{\boldsymbol{u}}_{00}\cdot\check{\nabla})\bar{\boldsymbol{u}}_{\phi}\right] - \beta\frac{\partial^2\tilde{p}_{01}}{\partial\check{z}^2}. \tag{5.38}$$

Eliminating $\tilde{\boldsymbol{u}}^{\perp}_{01}$ from (5.31*c*) and (5.32*a*), the boundary condition on $\mathscr{C}_0$ is

$$\hat{\boldsymbol{n}}^{\perp}\cdot\check{\nabla}\tilde{p}_{02} = \mathrm{i}\check{\omega}\beta H^{\mathrm{s}}_{Z}\left(G\tilde{w}_{01} - \tilde{U}^{\infty}_{01}\right) - \frac{\beta}{\lambda}\hat{\boldsymbol{n}}^{\perp}\cdot\left[(\tilde{\boldsymbol{u}}_{00}\cdot\check{\nabla})\bar{\boldsymbol{u}}^{\perp}_{\phi} + (\bar{\boldsymbol{u}}_{\phi}\cdot\check{\nabla})\tilde{\boldsymbol{u}}^{\perp}_{00}\right]. \tag{5.39}$$

As was the case for $\tilde{p}_{01}$ in § 5.3, the solution for $\tilde{p}_{02}$ can be determined only up to an additive function of $\check{z}$ at this point. Nevertheless, this is sufficient to recover $\tilde{\boldsymbol{u}}^{\perp}_{01}$ from (5.31*c*), so this completes the solution for the $O(\epsilon)$ flow in the core.

We note that knowledge of the leading-order mean flow $\bar{\boldsymbol{u}}_{\phi}$ is required to calculate the solution. Depending on the size of the oscillations relative to the other problem parameters, this will require the solution of either the problem described in § 4.2 or the problem described in § 7.1.

5.6. *The oscillatory flow in the Stokes layer at* $O(\epsilon)$

Corrections to the Stokes layer are necessary to match the $O(\epsilon)$ core flow to the velocity of the tube wall. The equations also contain forcing generated by the leading-order flow in the boundary layer in the form of the nonlinear Reynolds stresses and curvature-related terms. In addition, forcing from the leading-order flow enters via the linearization of the matching conditions between the core and the boundary layer.

As in the $O(1)$ case, the two transverse velocity components $\tilde{V}_{01}$ and $\tilde{W}_{01}$ smoothly match the core flows to the boundary conditions. The continuity equation is then solved to obtain the correction to the normal velocity $\tilde{\boldsymbol{u}}_{02}$. The details are omitted here, since the results are not required.

6. The higher-frequency oscillatory flow

The higher-frequency oscillatory flow $\hat{\boldsymbol{u}}$ is forced by products of lower-frequency quantities in two ways. First, the nonlinear inertia terms provide a non-zero forcing within the equations (see (3.4)). Second, the linearization of the boundary conditions on the wall and of the matching conditions between the core and the boundary layer results in non-zero boundary conditions on the higher-frequency components.

The size of each of these effects can be calculated, and hence the size of the response determined. The previously assumed scalings are confirmed as the correct choice, and hence the higher-frequency terms do not contribute to the leading-order steady and fundamental frequency terms. It is therefore unnecessary to consider the higher-frequency flow in any more detail.

7. Solution for the steady flow (part II)

Now that the first terms in the expansion of the oscillatory flow $\tilde{\boldsymbol{u}}$, $\tilde{p}$ have been calculated, we can return to the steady problem (first considered in § 4) and examine

the leading-order effects of the oscillations on the steady flow. As can be seen from (3.2), the contribution from the oscillatory flow comes in the form of an $O(\delta^2)$ Reynolds-stress term. As we shall see, this term is able to force velocities of $O(\delta^2/\epsilon)$ which may therefore be present at leading order. It is therefore necessary to consider at least the $O(\delta^0)$ and $O(\delta^2)$ terms together.

Since the oscillatory flow $\tilde{\boldsymbol{u}}_{00}$ has a boundary-layer structure, the forcing in, and hence the solution of, the steady equations is expected to have a similar boundary-layer structure. Fortunately, it is only necessary to examine the core flow in detail. Moreover, it is possible to introduce a modified pressure to absorb the additional Reynolds-stress term in the core. We write

$$\bar{\boldsymbol{u}}_0 + \delta^2 \bar{\boldsymbol{u}}_2 = \bar{\boldsymbol{u}}', \tag{7.1a}$$

$$\bar{p}_0 + \delta^2 \bar{p}_2 = \bar{\Pi} + \bar{p}', \tag{7.1b}$$

where

$$\left.\begin{aligned} \bar{\Pi}(\check{x}, \check{y}, \check{z}) &\equiv -\tfrac{1}{2}(\lambda\delta)^2 \epsilon\beta [\![|\tilde{\boldsymbol{u}}(\check{x}, \check{y}, \check{z}, \check{t})|^2 - |\tilde{\boldsymbol{u}}(0,0,0,\check{t})|^2]\!]_0 \\ &= -\tfrac{1}{4}(\lambda\delta)^2 (|\tilde{w}_{00}(\check{z})|^2 - |\tilde{w}_{00}(0)|^2) + O(\epsilon\delta^2, \delta^4). \end{aligned}\right\} \tag{7.2}$$

In the Stokes layer we use a similar expansion, but the pressure modification is chosen to match smoothly to the pressure in the core. As a result, it does not produce the exact cancellation with the Reynolds-stress term in the boundary-layer equations as we have in the core.

7.1. *The steady flow in the core*

Using the modified pressure, and neglecting the $O(\epsilon^2\delta^4)$ terms involving $\hat{\boldsymbol{u}}$, the equations (3.2) become

$$\check{\nabla}_\perp \cdot \bar{\boldsymbol{u}}'^{\perp} + \frac{\partial \bar{w}'}{\partial \check{z}} = 0, \tag{7.3a}$$

$$(\bar{\boldsymbol{u}}' \cdot \check{\nabla})\bar{\boldsymbol{u}}'^{\perp} = -\frac{1}{\epsilon\beta}\check{\nabla}_\perp \bar{p}' + \frac{\lambda\epsilon}{R^2}\check{\nabla}_\perp^2 \bar{\boldsymbol{u}}'^{\perp} + \frac{\lambda\beta\epsilon^2}{R^2}\frac{\partial^2 \bar{\boldsymbol{u}}'^{\perp}}{\partial \check{z}^2}, \tag{7.3b}$$

$$(\bar{\boldsymbol{u}}' \cdot \check{\nabla})\bar{w}' = -\frac{\partial \bar{p}'}{\partial \check{z}} + \frac{\lambda\epsilon}{R^2}\check{\nabla}_\perp^2 \bar{w}' + \frac{\lambda\beta\epsilon^2}{R^2}\frac{\partial^2 \bar{w}'}{\partial \check{z}^2}. \tag{7.3c}$$

Since the oscillatory flow is irrotational in the core, the pressure modification $\bar{\Pi}$ precisely cancels the additional Reynolds stress term from the oscillatory flow. Equations (7.3) for $(\bar{\boldsymbol{u}}', \bar{p}')$ are, therefore, identical to (4.3) for $(\bar{\boldsymbol{u}}_0, \bar{p}_0)$. The boundary conditions are slightly different however. The conditions at the tube ends are

$$\bar{p}' = 0 \quad \text{at} \quad \check{z} = 0 \tag{7.4a}$$

as before, and then either

$$\iint_{\mathscr{A}_0} \bar{w}' \, \mathrm{d}A = \pi \quad \text{at} \quad \check{z} = 1 \tag{7.4b}$$

if we are imposing a downstream flux condition, or

$$\bar{p}' = -\frac{\epsilon\lambda}{kR^2} - \tfrac{1}{4}(\lambda\delta)^2(|\tilde{w}_{00}(0)|^2 - |\tilde{w}_{00}(1)|^2) + O(\epsilon\delta^2, \epsilon^4) \quad \text{at} \quad \check{z} = 1 \tag{7.4c}$$

for a downstream pressure condition. The boundary condition to be applied to the velocity in the core on $\mathscr{W}_0$ also changes, as we must now take account of the boundary layer and the correct time-averaged linearization of the no-slip boundary condition. However, these turn out not to affect the $O(1)$ or $O(\delta^2)$ flow in the core (see § B.1) so can be neglected here to obtain a leading-order result. Formally, we find that

$$\bar{\boldsymbol{u}}' = \boldsymbol{0} + O(\epsilon\delta^2, \delta^4) \quad \text{on} \quad \mathscr{W}_0. \tag{7.4d}$$

For the case of pressure–flux boundary conditions, the equations and boundary conditions above are identical to those described in § 4 in the absence of any oscillations. Hence, to $O(\epsilon, \delta^2)$ the solution in the core is unchanged from the previous solution, save for the pressure change $\overline{\Pi}$ given in (7.2).

For the case of pressure–pressure boundary conditions, the downstream condition (7.4c) on the modified pressure is affected by the oscillations. The equations and other boundary conditions remain unchanged to $O(\epsilon, \delta^2)$, and so we now re-solve the system subject to an altered pressure difference between the tube ends. This will result in a difference between the flux $\mathscr{Q}_0$ in the absence of the oscillations and the flux $\mathscr{Q}_\phi$ with them. If the flux is proportional to the effective pressure difference, then we will have

$$\mathscr{Q}_\phi = \mathscr{Q}_0 \left[1 + \frac{\delta^2}{\epsilon} \frac{k\breve{\omega}^2 R^2 \lambda}{4} \left(\frac{|\tilde{\mathbb{V}}(0)|^2}{A_0(0)^2} - \frac{|\tilde{\mathbb{V}}(1)|^2}{A_0(1)^2} \right) \right], \tag{7.5}$$

and the change in flux will be $\mathscr{Q}_\phi - \mathscr{Q}_0 = O(\delta^2/\epsilon)$. This is the reason for the additional restriction $\delta^2 \lesssim \epsilon$, specified in § 2.5. The restriction is necessary to ensure that the mean axial flow in the presence of the oscillations still scales with $\mathscr{U}$.

7.2. *Boundary-layer and higher-order effects*

In the region occupied by the oscillatory boundary layers, the pressure modification $\overline{\Pi}$ no longer cancels the Reynolds stresses at leading order, and so $O(\delta^2)$ forcing terms appear in the tangential components of the momentum equation. There is also forcing at $O(\delta^2)$ from the linearization of the boundary condition on the tube wall. However, it turns out that this has no effect on the core flow at leading order, and the boundary condition (7.4d) used previously can indeed be applied.

The details of the calculations for the Stokes layer and consideration of other higher-order effects can be found in Appendix B.

8. The energy budget for periodic oscillations

In §§ 4–7 we constructed the leading-order terms in an asymptotic solution for the flow inside a tube undergoing prescribed oscillations. The solution uses the temporal decompositions (3.1) and (3.6), and series expansions in the small parameters ϵ and δ.

We now examine the energy budget corresponding to this leading-order solution. In particular, we determine the mean rate of working by the fluid on the tube walls, since this provides an indication of whether or not the oscillations would grow or decay if the external forcing were removed.

We re-write the energy equation (2.12) in terms of the dimensionless variables introduced in § 2.4. After taking the steady component, we obtain

$$\underbrace{\left[\!\left[\left[\iint_{\mathscr{A}} \frac{1}{2}(\check{w}^2+\epsilon\beta|\check{\boldsymbol{u}}^{\perp}|^2)\check{w}\,\mathrm{d}A\right]_{\check{z}=1}^{\check{z}=0}\right]\!\right]_0}_{\mathscr{K}} - \underbrace{\left[\!\left[\frac{\lambda}{\epsilon}\left[\iint_{\mathscr{A}} \check{w}\check{p} - \frac{2\epsilon^2}{R^2}\left(\check{\boldsymbol{u}}\cdot\check{\mathbf{e}}\cdot\hat{\boldsymbol{z}}\right)\mathrm{d}A\right]_{\check{z}=0}^{\check{z}=1}\right]\!\right]_0}_{\mathscr{S}}$$
$$- \underbrace{\left[\!\left[\frac{\lambda}{\epsilon}\iint_{\mathscr{W}} \check{p}\,\check{\boldsymbol{u}}\cdot\hat{\boldsymbol{N}} - \frac{2\epsilon^2}{R^2}\left(\frac{1}{\ell}\check{\boldsymbol{u}}\cdot\check{\mathbf{e}}\cdot\hat{\boldsymbol{N}}\right)\mathrm{d}S\right]\!\right]_0}_{\mathscr{E}} - \underbrace{\left[\!\left[\frac{\epsilon\lambda}{R^2}\iiint_{\mathscr{V}} 2\,\check{\mathbf{e}}:\check{\mathbf{e}}\,\mathrm{d}V\right]\!\right]_0}_{\mathscr{D}} = 0, \tag{8.1}$$

where

$$\check{\mathbf{e}} = \frac{1}{2\ell}\left[\check{\boldsymbol{\nabla}}\check{\boldsymbol{u}} + (\check{\boldsymbol{\nabla}}\check{\boldsymbol{u}})^{\mathrm{T}}\right] \tag{8.2}$$

is the non-dimensional rate of strain tensor, which, following (3.1), can be decomposed as

$$\check{\mathbf{e}} = \bar{\mathbf{e}} + \lambda\delta\tilde{\mathbf{e}} + \lambda\delta\epsilon^2\hat{\mathbf{e}}, \tag{8.3}$$

into steady, fundamental oscillatory and higher frequency components in the same way as the other variables.

We introduce $\mathscr{K}$, $\mathscr{S}$, $\mathscr{E}$ and $\mathscr{D}$ to represent the various time-averaged (dimensionless) energy fluxes as indicated in (8.1). Each of these energy fluxes is non-dimensionalized on

$$\rho\mathscr{U}^3a^2, \tag{8.4}$$

chosen to match the steady flux of kinetic energy from the background flow. The energy budget (8.1) can then be written as

$$\mathscr{E} = \mathscr{K} - \mathscr{S} - \mathscr{D}. \tag{8.5}$$

Physically, $\mathscr{K}$ is the time-averaged net kinetic energy influx from the tube ends, $\mathscr{S}$ is the time-averaged rate of working of fluid at the tube ends, $\mathscr{E}$ is the time-averaged rate of working done by fluid on the tube walls and $\mathscr{D}$ is the time-averaged rate of dissipation.

We will now evaluate these four energies and, in particular, the energy transfer to the wall $\mathscr{E}$. Since we were unable to write down a closed-form solution for the steady flow even at leading order, we cannot evaluate the contributions from the steady flow. However, it will turn out that the problematic terms cancel amongst themselves by virtue of the steady system satisfying a separate energy equation. We exploit this fact to derive the leading-order energy budget for the oscillatory components of the system.

Since the $(\bar{\boldsymbol{u}}', \bar{p}')$ system described in § 7.1 also satisfies the Navier–Stokes equations at leading order, we can also construct a similar energy balance with $(\check{\boldsymbol{u}}, \check{p})$ in (8.1) replaced by $(\bar{\boldsymbol{u}}', \epsilon\bar{p}'/\lambda)$. (The factor multiplying $\bar{p}'$ is a consequence of the decomposition (3.1*b*).) We denote the corresponding steady fluxes by $\mathscr{E}'$, $\mathscr{S}'$, $\mathscr{K}'$ and $\mathscr{D}'$. Equation (7.4*d*) shows that in the $(\bar{\boldsymbol{u}}', \bar{p}')$ system the normal velocity at the wall is zero at leading order, and so we have

$$\mathscr{K}' - \mathscr{S}' - \mathscr{D}' = O(\epsilon^2, \epsilon\delta^2, \delta^4). \tag{8.6}$$

We now express each of the variables in the full energy equation (8.1) in terms of the temporal decomposition (3.1), keeping terms up to $O(\delta^2)$. We also express the steady

components using the decomposition (7.1). Each of the four time-averaged energy contributions can then be expressed as the sum of its $(\bar{\boldsymbol{u}}', \bar{p}')$ counterpart and an expansion in powers of ϵ and δ. It will be sufficient to evaluate just the leading-order term in the expansion for each flux.

8.1. *The kinetic energy flux through the tube ends*

Using the decomposition (3.1) and the modified steady state defined in (7.1), the time-averaged net influx of kinetic energy flux through the tube ends is given by

$$\mathscr{K} = \frac{1}{2}\left[\iint_{\mathscr{A}_0} \bar{w}'\left(\bar{w}'^2 + \epsilon\beta|\bar{\boldsymbol{u}}'^{\perp}|^2\right)\mathrm{d}A\right]_{\check{z}=1}^{\check{z}=0} + \frac{1}{2}(\lambda\delta)^2\left[\iint_{\mathscr{A}_0} 3\bar{w}'[\![\tilde{w}^2]\!]_0\,\mathrm{d}A\right]_{\check{z}=1}^{\check{z}=0} + O(\epsilon^2, \epsilon\delta^2, \delta^4). \quad (8.7)$$

The equivalent flux for the $(\bar{\boldsymbol{u}}', \bar{p}')$ system is

$$\mathscr{K}' = \frac{1}{2}\left[\iint_{\mathscr{A}_0} \bar{w}'\left(\bar{w}'^2 + \epsilon\beta|\bar{\boldsymbol{u}}'^{\perp}|^2\right)\mathrm{d}A\right]_{\check{z}=1}^{\check{z}=0}. \quad (8.8)$$

We observe that $\mathscr{K}$ and $\mathscr{K}'$ differ only by $O(\delta^2)$, and hence we write

$$\mathscr{K} = \mathscr{K}' + \delta^2\mathscr{K}_2 + O(\epsilon^2, \epsilon\delta^2, \delta^4), \quad (8.9)$$

where

$$\mathscr{K}_2 = \frac{3\lambda^2}{4}\left[\iint_{\mathscr{A}_0} \bar{w}'|\tilde{w}_{00}|^2\,\mathrm{d}A\right]_{\check{z}=1}^{\check{z}=0}. \quad (8.10)$$

Physically, $\mathscr{K}'$ arises due to any acceleration or deceleration of the mean flow along the length of the tube. The second term $\mathscr{K}_2$ arises from the non-zero mean of the square of the axial sloshing flow at the inlet.

To evaluate $\mathscr{K}_2$, we note that $\tilde{w}_{00}$ is uniform in the core of each cross-section, and so we can evaluate the integral directly using (4.8). We obtain

$$\mathscr{K}_2 = \frac{3\lambda^2\mathscr{Q}_\Phi}{4}\left[|\tilde{w}_{00}|^2\right]_{\check{z}=1}^{\check{z}=0} = \frac{3\lambda^2\check{\omega}^2\mathscr{Q}_\Phi}{4}\left(\frac{|\tilde{\mathbb{V}}(0)|^2}{A_0(0)^2} - \frac{|\tilde{\mathbb{V}}(1)|^2}{A_0(1)^2}\right), \quad (8.11)$$

where we have eliminated $\tilde{w}$ in favour of $\tilde{\mathbb{V}}$ using (5.13*a*).

8.2. *The work done by the fluid at the tube ends*

The mean rate of working by the fluid at the ends of the tube is dominated by the pressure term acting over the core region. We have

$$\mathscr{S} = \left[\iint_{\mathscr{A}_0}\left(\bar{w}'(\bar{p}' + \overline{\Pi}) + \frac{\lambda^3\delta^2}{\epsilon}[\![\tilde{w}\tilde{p}]\!]_0\right)\mathrm{d}A\right]_{\check{z}=0}^{\check{z}=1} + O(\epsilon^2, \epsilon\delta^2, \delta^4). \quad (8.12)$$

The contribution from the $\tilde{w}\tilde{p}$ term is at most $O(\epsilon\delta^2)$: at an end with a pressure condition, we have $\tilde{p} = 0$ so there is no contribution from that end at all; at an end with a flux condition, then the facts that $\tilde{w}_{00} = 0$, $\iint \tilde{w}_{01}\,\mathrm{d}A = 0$ and $\nabla_\perp\tilde{p}_{00} = 0$ ensure that the $O(1)$ and $O(\epsilon)$ contributions from $\tilde{w}\tilde{p}$ vanish.

The equivalent expression to (8.12) for the $(\bar{\boldsymbol{u}}', \bar{p}')$ system is

$$\mathscr{S}' = \left[\iint_{\mathscr{A}_0} \bar{w}'\bar{p}'\,\mathrm{d}A\right]_{\check{z}=0}^{\check{z}=1} + O(\epsilon^2, \epsilon\delta^2, \delta^4). \quad (8.13)$$

From (7.2), we have that $\overline{\Pi} = \delta^2 \overline{\Pi}_2(\check{z}) + O(\epsilon\delta^2, \delta^4)$, where

$$\overline{\Pi}_2(\check{z}) \equiv -\frac{\lambda^2}{4}(|\tilde{w}_{00}(\check{z})|^2 - |\tilde{w}_{00}(0)|^2), \tag{8.14}$$

and so $\mathscr{S}$ and $\mathscr{S}'$ differ by an $O(\delta^2)$ amount. We therefore write

$$\mathscr{S} = \mathscr{S}' + \delta^2 \mathscr{S}_2 + O(\epsilon^2, \epsilon\delta^2, \delta^4), \tag{8.15}$$

where

$$\mathscr{S}_2 = \left[\iint_{\mathscr{A}_0} \bar{w}' \overline{\Pi}_2 \, \mathrm{d}A \right]_{\check{z}=0}^{\check{z}=1}. \tag{8.16}$$

Substituting for $\overline{\Pi}_2$ from (8.14) and using (4.8) and (5.13*a*), we obtain

$$\mathscr{S}_2 = \frac{\check{\omega}^2 \lambda^2 \mathbb{Q}_0}{4} \left(\frac{|\tilde{\mathbb{V}}(0)|^2}{A_0(0)^2} - \frac{|\tilde{\mathbb{V}}(1)|^2}{A_0(1)^2} \right). \tag{8.17}$$

Physically, $\mathscr{S}'$ represents the work done by the $(\bar{\boldsymbol{u}}', \bar{p}')$ system itself, while $\mathscr{S}_2$ is the leading-order work done by the combination of the mean flow $\bar{\boldsymbol{u}}'$ and the pressure gradient $\overline{\Pi}$ due to the Reynolds stresses from the oscillatory flow. The steady boundary conditions at the tube ends mean that there is no direct contribution from the oscillatory flow.

8.3. *The dissipation in the Stokes layer and the core*

The dissipation is given by the local dissipation integrated over the whole volume. Linearizing to the mean volume incurs only $O(\epsilon^2\delta^2)$ errors, so we arrive at

$$\mathscr{D} = \frac{2\epsilon\lambda}{R^2} \iiint_{\mathscr{V}_0} \left(\bar{\mathbf{e}}' : \bar{\mathbf{e}}' + (\lambda\delta)^2 [\![\tilde{\mathbf{e}} : \tilde{\mathbf{e}}]\!]_0 \right) \mathrm{d}V + O(\epsilon^2, \epsilon\delta^2, \delta^4). \tag{8.18}$$

The corresponding expression for the $(\bar{\boldsymbol{u}}', \bar{p}')$ system is

$$\mathscr{D}' \equiv \frac{2\epsilon\lambda}{R^2} \iiint_{\mathscr{V}_0} \bar{\mathbf{e}}' : \bar{\mathbf{e}}' \, \mathrm{d}V + O(\epsilon^2, \epsilon\delta^2, \delta^4). \tag{8.19}$$

As before, there is an $O(\delta^2)$ difference, and we write

$$\mathscr{D} = \mathscr{D}' + \delta^2 \mathscr{D}_2 + O(\epsilon^2, \epsilon\delta^2, \delta^4). \tag{8.20}$$

The leading-order dissipation from the oscillatory flow occurs in the Stokes layer adjacent to the wall. (The dissipation in the core is smaller by a factor of $O(\epsilon)$.) Since the layer is thin and axial velocities are larger than tangential velocities, the leading-order component of the rate-of-strain tensor comes from the normal gradient of the axial velocity. We, therefore, have

$$\mathscr{D}_2 \equiv \frac{\lambda^3}{4R^2} \iint_{\mathscr{W}_0} \int_0^\infty \left| \frac{\partial \tilde{W}_{00}}{\partial \check{X}} \right|^2 \mathrm{d}\check{X} \, \mathrm{d}S. \tag{8.21}$$

From (5.27*b*), the leading-order axial velocity in the Stokes layer can be written in terms of $\tilde{w}_{00}$ at the outer edge of the core. From this, we obtain

$$\left| \frac{\partial \tilde{W}_{00}}{\partial \check{X}} \right| = \tilde{w}_{00}|_{\mathscr{C}_0} \, \check{\omega}^{1/2} R \, \exp\{-(\check{\omega}/2)^{1/2} R \, \check{X}\}, \tag{8.22}$$

and hence

$$\mathscr{D}_2 = \frac{\check{\omega}^{1/2}\lambda^3}{2\sqrt{2}\,R} \iint_{\mathscr{W}_0} |\tilde{w}_{00}|^2 \, \mathrm{d}S = \frac{\check{\omega}^{5/2}\lambda^3}{2\sqrt{2}\,R} \int_0^1 \oint_{\mathscr{C}_0(\check{z})} \frac{|\tilde{\mathbb{V}}(\check{z})|^2}{A_0(\check{z})^2} H_Y^{\mathrm{s}} H_Z^{\mathrm{s}} \, \mathrm{d}\check{Y} \, \mathrm{d}\check{z}. \tag{8.23}$$

There is an implicit assumption here that the flow $\tilde{w}_{00}$ is $O(1)$ over a significant portion of the tube, so that the $\partial \tilde{W}_{00}/\partial X$ term in the rate-of-strain tensor does indeed provide the dominant contribution to the dissipation. In particular, this restriction excludes deformations that result in no area change at leading order (e.g. the non-axisymmetric normal modes of an elastic circular cylinder).

8.4. *The work done by the fluid on tube walls*

We decompose $\mathscr{E}$ in a similar manner to the other fluxes, writing

$$\mathscr{E} = \mathscr{E}' + \delta^2 \mathscr{E}_2 + O(\epsilon^2, \epsilon\delta^2, \delta^4), \tag{8.24}$$

where $\mathscr{E}'$ is the time-averaged energy flux in the $(\bar{\boldsymbol{u}}', \bar{p})$ system. As already noted, $\mathscr{E}'$ may be neglected at the orders in which we are interested, since the normal velocity in the $(\boldsymbol{u}', p')$ system is sufficiently small at the wall.

Starting from the energy balance (8.5), we can use the decompositions (8.9), (8.15), (8.20) and (8.24) to express each term in terms of the corresponding term from the $(\bar{\boldsymbol{u}}', \bar{p})$ system, the δ^2 correction and higher-order errors. From (8.6) the sum of the $(\bar{\boldsymbol{u}}', \bar{p})$ terms is negligible, and we are left with

$$\mathscr{E}_2 = \mathscr{K}_2 - \mathscr{S}_2 - \mathscr{D}_2 \tag{8.25}$$

as the leading-order balance. Equivalently, $\mathscr{E}$ may be evaluated by direct calculation of the work done on the wall, and this method does indeed give the same answer (details omitted for brevity).

Examining the values of $\mathscr{K}_2$ in (8.11) and $\mathscr{S}_2$ in (8.17), the expression for the energy may also be written as

$$\mathscr{E} = \delta^2 \mathscr{E}_2 = \delta^2 \left(\frac{2}{3} \mathscr{K}_2 - \mathscr{D}_2 \right). \tag{8.26}$$

The time-averaged work on the wall comprises an input of $2\delta^2 \mathscr{K}_2/3$ due to the axial oscillatory velocity at the tube ends, minus dissipative losses of $\delta^2 \mathscr{D}_2$ from the Stokes layer. Of the total kinetic energy input $\delta^2 \mathscr{K}_2$, only 2/3 is available to do work on the wall. The other 1/3 goes into the $(\bar{\boldsymbol{u}}', \bar{p})$ system and is lost either as dissipation from an increased mean flow (pressure–pressure conditions) or as additional work against an increased mean pressure gradient (flux–pressure conditions). Interestingly, the 2 : 1 partition is the same as that seen by Jensen & Heil (2003) in their analysis of a two-dimensional channel with pressure boundary conditions at both ends.

Observe that (8.25) could not simply be obtained by equating the $O(\delta^2)$ terms in the full energy balance (8.5), since there are also some $O(\delta^2)$ terms present in the $(\bar{\boldsymbol{u}}', \bar{p}')$ system and its energy equation (8.6).

9. Neutral energy condition and interpretation

9.1. *The critical inverse Strouhal number*

We now consider the implications of the expression (8.25) for the leading-order time-averaged energy flux from the fluid to the wall. We substitute in the expressions (8.11), (8.17) and (8.21) for the fluxes $\mathscr{K}_2$, $\mathscr{S}_2$ and $\mathscr{D}_2$. After a little rearrangement, we obtain

$$\mathscr{E}_2 = \frac{\check{\omega}^2 \lambda^2 \mathbb{Q}_\phi}{2} \frac{|\tilde{\mathbb{V}}(0)|^2}{A_0(0)^2} \left[\left(1 - \frac{|\tilde{\mathbb{V}}(1)|^2}{|\tilde{\mathbb{V}}(0)|^2} \frac{A_0(0)^2}{A_0(1)^2} \right) - \frac{\lambda}{R\mathbb{Q}_\phi} (2\pi\check{\omega} A_0(0))^{1/2} I \right], \tag{9.1}$$

where

$$I \equiv \int_0^1 \left\{ \mathbb{P}(\check{z}) \frac{A_0(0)^{3/2}}{A_0(\check{z})^{3/2}} \frac{|\tilde{\mathbb{V}}(\check{z})|^2}{|\tilde{\mathbb{V}}(0)|^2} \right\} \mathrm{d}\check{z}, \tag{9.2}$$

and

$$\mathbb{P}(\check{z}) \equiv \frac{1}{2\pi^{1/2} A_0(\check{z})^{1/2}} \oint_{\mathscr{C}_0(\check{z})} H_Y^{\mathrm{s}} H_Z^{\mathrm{s}} \, \mathrm{d}Y \tag{9.3}$$

is a 'shape factor', giving the ratio of the surface area between $\check{z}$ and $\check{z} + \mathrm{d}\check{z}$ to that of a circular cylinder with the same cross-sectional area $A_0(\check{z})$, in the limit as $\mathrm{d}\check{z} \to 0$.

Recalling that $\mathscr{E} = \delta^2 \mathscr{E}_2$, and rewriting (λ, R, δ) in terms of (α, ℓ, St), we obtain

$$\mathscr{E} = \frac{\check{\omega}^2 \Delta^2 \ell^2 St^2 \mathbb{Q}_{\phi}}{2} \frac{|\tilde{\mathbb{V}}(0)|^2}{A_0(0)^2} \left[\left(1 - \frac{|\tilde{\mathbb{V}}(1)|^2}{|\tilde{\mathbb{V}}(0)|^2} \frac{A_0(0)^2}{A_0(1)^2} \right) - \frac{\ell St}{\alpha \mathbb{Q}_{\phi}} (2\pi \check{\omega} A_0(0))^{1/2} I \right]. \tag{9.4}$$

The condition $\mathscr{E} = 0$ can be used to define a criticality condition, in terms of a critical inverse Strouhal number St_c^{-1}, at which there is zero time-averaged energy transfer to the wall. In terms of the unscaled dimensionless groups introduced in (2.22), we find that

$$\frac{1}{St_c} = \frac{\ell}{\alpha \mathbb{Q}_{\phi}} (2\pi \check{\omega} A_0(0))^{1/2} \left(1 - \frac{|\tilde{\mathbb{V}}(1)|^2 A_0(0)^2}{|\tilde{\mathbb{V}}(0)|^2 A_0(1)^2} \right)^{-1} \int_0^1 \left\{ \mathbb{P}(\check{z}) \frac{A_0(0)^{3/2}}{A_0(\check{z})^{3/2}} \frac{|\tilde{\mathbb{V}}(\check{z})|^2}{|\tilde{\mathbb{V}}(0)|^2} \right\} \mathrm{d}\check{z}. \tag{9.5}$$

Recall that ℓ and α are the aspect ratio and Womersley number defined in (2.22); $A_0(\check{z})$ is the cross-sectional area of the tube in the steady configuration; $\mathbb{Q}_{\phi}$ is the dimensionless steady flux defined in (4.8); $\mathbb{P}(\check{z})$ is the shape factor defined in (9.3); and $\tilde{\mathbb{V}}(\check{z})$ is the effective volume change due to the oscillations, as defined in (5.16). Observe that $\mathbb{P}(\check{z})$ and $A_0(\check{z})$ are simply functions of the geometry of the steady configuration, and that the only additional information required to calculate $\tilde{\mathbb{V}}(\check{z})$ is the oscillatory change in cross-sectional area $\tilde{A}(\check{z})$.

For pressure–pressure conditions and $\delta^2 \sim \epsilon$, the oscillations have a leading-order effect on $\mathbb{Q}$ (i.e. $\mathbb{Q}_{\phi} \neq \mathbb{Q}_0$). Then $\mathbb{Q}_{\phi}$ will, in general, have a dependence on St, and (9.5) must be manipulated further to obtain a closed-form expression for St_c. For example, for the case of a tube whose undeformed configuration is axially uniform, the change in flux will be given by (7.5), which we can rewrite as

$$\mathbb{Q}_{\phi} = \mathbb{Q}_0 (1 + \Psi St), \tag{9.6}$$

where we have introduced

$$\Psi = \frac{k \check{\omega}^2 \alpha^2 \ell \Delta^2}{4 A_0^2} \left(|\tilde{\mathbb{V}}(0)|^2 - |\tilde{\mathbb{V}}(1)|^2 \right). \tag{9.7}$$

The criticality condition (9.5) can then be expressed as

$$\frac{1}{St_c} = \frac{\ell}{\alpha \mathbb{Q}_0} \frac{(2\pi \check{\omega} A_0)^{1/2}}{|\tilde{\mathbb{V}}(0)|^2 - |\tilde{\mathbb{V}}(1)|^2} \int_0^1 \mathbb{P}(\check{z}) |\tilde{\mathbb{V}}(\check{z})|^2 \, \mathrm{d}\check{z} - \Psi. \tag{9.8}$$

With pressure–flux boundary conditions and also for pressure–pressure conditions when $\delta^2 \ll \epsilon$ (i.e. when $\mathbb{Q}_{\phi} = \mathbb{Q}_0$ to leading order), (9.8) still applies, but with $\Psi = 0$.

When $\mathbb{Q}_{\phi} = \mathbb{Q}_0$, condition (9.5) is independent of the amplitude of the oscillations (although its derivation requires them to be small, which is appropriate for an analysis of the *onset* of self-excited oscillations), and the overall length of the tube enters only through the single factor ℓ.

As $St^{-1} \propto \mathscr{U}$, this parameter can be thought of as a dimensionless strength of the background flow. For $St^{-1} < St_c^{-1}$, energy is being supplied by the wall to maintain the motion, so the system is stable to such oscillations. For $St^{-1} > St_c^{-1}$ we have a mean transfer of energy to the wall, suggesting that an instability may be possible.

9.2. *Physical interpretation*

Examining (9.5), we can decrease St_c^{-1}, and hence reduce the flow rate at which self-excited oscillations are likely to develop, by one or more of the following procedures:

(i) decreasing the value of the group $\ell(\check{\omega}A_0(0))^{1/2}/(\alpha\mathbb{Q}_\phi)$;

(ii) choosing a cross-sectional shape for the tube so as to reduce the relative perimeter $\mathbb{P}(\check{z})$;

(iii) increasing the cross-sectional area $A_0(\check{z})$ over most of the tube, relative to its value $A_0(0)$ at the upstream end;

(iv) localizing the disturbance near the upstream ($\check{z} = 0$) end, so that $|\tilde{\mathbb{V}}(\check{z})/\tilde{\mathbb{V}}(0)|$ is smaller over a greater proportion of the interval $[0, 1]$ (e.g. by adjusting the lengths of any upstream and downstream rigid sections);

(v) ensuring that the changes in cross-sectional area at different axial locations are more in phase with each other, so that contributions to $|\tilde{\mathbb{V}}(\check{z})|$ within the tube also contribute to $|\tilde{\mathbb{V}}(0)|$ at the end;

(vi) in the case of pressure–pressure conditions, having $A_0(1)$ large relative to $A_0(0)$, which helps to minimize kinetic energy losses from the downstream end.

Item (i) serves to alter the dimensional scalings to decrease the relative strength of the dissipative term relative to the energy input term. For example, consider the dependence of tube length ℓ. The oscillatory energy input scales with the square of the size of the oscillations in the volume of the tube, which is proportional to ℓ^2. The dissipation scales with the square of the size of the oscillations (ℓ^2), and also with the volume of the Stokes layers, which is proportional to ℓ. Hence, increasing the tube length reduces the energy transfer to the wall, thus making the development of an instability less likely.

The scaling with the Womersley number α^2 arises purely from the dissipative term. The dissipation scales like the product of viscosity, the square of the velocity gradients and the volume of the Stokes layers. The first factor scales like α^{-2}, while the second and third depend on the thickness of the Stokes layers raised to the -2 and $+1$ powers, respectively. The thickness of the Stokes layer scales like α^{-1}, hence there is an overall factor of α^{-1} in St_c^{-1}.

The other items (ii)–(vi) reduce the dimensionless viscous losses relative to the kinetic energy input. Item (ii) reduces the volume of the Stokes layer by minimizing the tube perimeter at each cross-section. (We note that this result does not contradict Heil & Waters' (2008) finding that the instability mechanism ceases to operate efficiently for small-amplitude oscillations of circular cylindrical tubes, even though such tubes have the smallest possible relative perimeter. This is because natural oscillations about a circular cross-section are a special case and behave differently, for the reasons described in § 9.3.) Items (iii) and (iv) reduce the axial sloshing flow (and hence the dissipation it causes) over as much of the tube as possible, relative to that at the inlet (which is responsible for the energy input). Item (v) arises from the fact that if the wall motion at different points is not in phase, then the amplitude of the oscillations in the tube volume, and hence of the sloshing flows seen at the ends, is reduced. Item (vi) increases the net input of kinetic energy by reducing the relative losses at the downstream end.

9.3. *Limits of validity and pathological cases*

The expression (9.5) is valid provided the various parameters (including the predicted St_c^{-1}) are within the asymptotic regime defined in § 2.5. There is one exception.

If $\tilde{\mathbf{V}}(\tilde{z}) = 0$ or is small over most of the tube, then neglected higher-order effects may dominate. The dissipation is assumed to be dominated by the flow in the Stokes boundary layer that is induced by the oscillatory axial plug flow in the core. If this oscillatory flow in the boundary layer has a small amplitude over much of the tube, then the leading-order dissipation could come from higher-order effects (for instance, dissipation due to the cross-sectional flow), which were neglected in the analysis. More precisely, we require that the integral in (9.5) be $O(1)$ as $\epsilon \to 0$ to ensure that the dissipation is dominated by the assumed terms.

This case also includes the situation in which the tube has a circular cross-section in the undeformed configuration. Natural small-amplitude deformations of a circle with dimensionless amplitude Δ result in changes to the cross-sectional area only of $O(\Delta^2)$. Since we only consider changes that are linear in the displacement amplitude, we would find that $\tilde{\mathbf{V}} \equiv 0$. With the axial sloshing flows only of $O(\Delta^2)$ the dissipation in the Stokes layers is reduced, and dissipation due to the flow in the cross-section becomes significant. The effect of this additional contribution to the dissipation is sufficient to dominate the effect (ii) in § 9.2. Therefore, even though a circular cross-section has the smallest relative perimeter, the instability mechanism does not operate as effectively there. This is consistent with the findings of Heil & Waters (2008).

There are two other cases that may appear problematic looking at (9.5), but in fact are not. First, when

$$\frac{|\tilde{\mathbf{V}}(0)|}{A_0(0)} = \frac{|\tilde{\mathbf{V}}(1)|}{A_0(1)}, \tag{9.9}$$

the denominator on the right-hand side of (9.5) vanishes. In this case, the kinetic energy fluxes at the two ends of the tube are equal at leading order, and there is no net influx of energy. Therefore, dissipative losses dominate and there must be a net transfer of energy from the wall to the flow in order to sustain the oscillations. An infinite critical inverse Strouhal number is therefore predicted. In general, higher-order effects will result in a small positive or negative influx of kinetic energy, yielding a large yet finite critical inverse Strouhal number. However, such values of St are outside the range of validity of the theory, and the energy transfer is correctly predicted for $\epsilon \ell St = O(1)$.

Finally, observe that the limit $\tilde{\mathbf{V}}(0) = 0$ is not singular, and with a little rearrangement, expression (9.5) can still be used. However, with no kinetic energy flux at the upstream end, a negative critical Strouhal number (corresponding to a negative mean flow) will be predicted. In other words, the flow must be reversed, interchanging the effective upstream and downstream ends, for the instability to manifest itself.

10. Conclusions

We have constructed an asymptotic solution for the flow through an oscillating tube with a prescribed wall motion and a background axial flow induced by either flux or pressure conditions at the tube ends. The solution applies to an arbitrary initial tube shape and harmonic oscillation mode but is restricted to tubes with an axially slowly varying shape, a small-amplitude high-frequency oscillation and the parameter values satisfying (2.27), a regime chosen to include the case of energetically neutral oscillations (see § 2.5).

Using these results, we derived an expression (9.1) for the time-averaged energy transfer from the fluid to the wall. We postulate that the sign of this energy transfer is associated with the stability of the system to free oscillations. We obtained a simple expression (9.5) that describes the critical case of oscillations with a neutral energy budget. The scaling $St_c^{-1} \propto \alpha$ is consistent with the results of Heil & Waters (2008), who used scaling arguments to obtain the functional relationship between these two quantities. In addition, as will be shown in Part 2 of this paper (Whittaker *et al.* 2010), our asymptotic results show excellent agreement with numerical simulations of a fully three-dimensional flow.

Our analysis shows that the instability mechanism proposed by Jensen & Heil (2003) for two-dimensional flows (and described briefly in the introduction) also applies to three-dimensional tubes. The partition of the additional kinetic energy input due to the oscillations remains exactly 2 : 1 between the energy that is available to do work on the walls and the energy that is lost because of changes in the steady flow, as in the two-dimensional case. More surprisingly, the same 2 : 1 partition is seen to hold, at least approximately, in a one-dimensional model of two-dimensional channel flow in a regime without the presence of Stokes layers (Stewart, Waters & Jensen 2009). We anticipate that this common partition can be explained more generally, and this will be addressed in future work.

We stress that the energy transfer criterion is not identical to the actual stability criterion for free oscillations involving full fluid–structure interaction. Part of the excess energy that is transmitted to the walls in the case of prescribed constant-amplitude oscillations would instead be required to increase the kinetic energy of the fluid in order to increase the amplitude of free oscillations. Therefore, more complex interactions may need to be considered. Nevertheless, the results presented in this paper provide an essential ingredient in the understanding of the physical mechanisms underlying a particular global instability of flows through a collapsible tube. The key result (9.5) also provides a remarkably simple stability criterion that can be applied to any observed or postulated mode shape. The extension of this work to the full fluid–structure interaction problem for free oscillations is currently in progress.

We note that the instability mechanism that applies in the regime studied here requires the flow to be oscillatory at the upstream end of the tube in order to allow additional energy into the system. This contrasts with the case studied by Luo & Pedley (1996), Luo *et al.* (2008) and many others, in which a flux condition is applied at the upstream end of the tube, so that the oscillatory flow is zero there. With such a set-up, the net kinetic energy flux from the two ends will be negative in the presence of oscillations, since the oscillatory flow at the downstream end will increase the outflux there. Therefore, a different mechanism is required to provide the energy to drive the instability in this case.

The mechanism that we have studied in this paper involves the extraction of energy from the external agent that is maintaining boundary conditions to induce the steady background flow. The increased mean kinetic energy flux $\mathscr{K}$ means that more work must be done at the tube ends to maintain the assumed boundary conditions. We note that the presence of dissipation is not a prerequisite for the instability, and the mechanism persists as $\mu \to 0$.

It is possible to generalize our results to the case where the oscillation amplitude is still small, but no longer much smaller than the width of the Stokes layer. To describe such a flow, the boundary-layer coordinates must move and deform with the boundary, leading to more complicated equations and matching conditions. Nevertheless, since the motion of the layer is small, inertial and divergence effects are also small, and at

leading order the form of the solution is unaffected. This will be presented in a future paper.

The authors would like to acknowledge the financial support of the Engineering and Physical Sciences Research Council to undertake the project of which this work is a part. R. J. W. and S. L. W. are supported by grant EP/D070910/2; M. H. and J. B. are supported by grant EP/D670422/1. S. L. W. is also is grateful to the EPSRC for funding in the form of an Advanced Research Fellowship. Helpful conversations with Peter Stewart are also gratefully acknowledged.

Appendix A. Coordinates and equations for the Stokes layer

In this appendix, we define the coordinate system and variables used to describe the flow in the Stokes boundary layers adjacent to the tube walls and derive the appropriate governing equations and boundary conditions.

A.1. *Coordinate system*

We use the previously introduced dimensionless surface coordinates $(\check{Y}, \check{Z})$ to which we add a normal coordinate $\check{X}$, as illustrated in figure 4. The surface $\check{X} = 0$ coincides with the tube wall in the steady configuration. The $\check{X}$ coordinate is scaled with the boundary-layer thickness ϵ, so that the dimensionless position vector $\check{\boldsymbol{r}}$ of the point $(\check{X}, \check{Y}, \check{Z})$ is related to that of the corresponding point $\check{\boldsymbol{r}}_0$ at $(0, \check{Y}, \check{Z})$ on the wall in the steady configuration by

$$\check{\boldsymbol{r}}(\check{X}, \check{Y}, \check{Z}) = \check{\boldsymbol{r}}_0(\check{Y}, \check{Z}) - \epsilon\, \check{X}\, \hat{\boldsymbol{n}}(\check{Y}, \check{Z}). \tag{A 1}$$

Derivatives of a general dimensional position vector $\boldsymbol{r}$ relate the coordinates to the unit vectors. Following (2.4), we write

$$\frac{\partial \check{\boldsymbol{r}}}{\partial \check{X}} = -\epsilon \hat{\boldsymbol{n}}\,, \quad \frac{\partial \check{\boldsymbol{r}}}{\partial \check{Y}} = H_Y(\check{X}, \check{Y}, \check{Z})\hat{\boldsymbol{t}}, \quad \frac{\partial \check{\boldsymbol{r}}}{\partial \check{Z}} = \ell\, H_Z(\check{X}, \check{Y}, \check{Z})\hat{\boldsymbol{b}}, \tag{A 2a–c}$$

where H_Y and H_Z are the dimensionless scale factors. Substituting (A 1) into (A 2), we obtain

$$H_Y(\check{X}, \check{Y}, \check{Z}) = H_Y^{\mathrm{s}}(\check{Y}, \check{Z}) - \epsilon\, \check{K}_Y\, \check{X}, \tag{A 3a}$$

$$H_Z(\check{X}, \check{Y}, \check{Z}) = H_Z^{\mathrm{s}}(\check{Y}, \check{Z}) - \epsilon^2 \beta\, \check{K}_Z\, \check{X}, \tag{A 3b}$$

where H_Y^{s} and H_Z^{s} are the scale factors for the surface coordinates that were defined in (2.4), $\check{K}_Y$ and $\check{K}_Z$ are two of the dimensionless curvatures introduced through (2.6) and (2.26) and β is defined in (2.31c).

A.2. *Navier–Stokes equations*

The (dimensional) fluid velocity $\check{\boldsymbol{U}}$ in the boundary layer is decomposed into components aligned with the unit vectors corresponding to the boundary-layer coordinates, thus

$$\check{\boldsymbol{u}} = \check{\boldsymbol{U}} \equiv \check{U}\hat{\boldsymbol{n}} + \check{V}\hat{\boldsymbol{t}} + \ell \check{W}\hat{\boldsymbol{b}}. \tag{A 4}$$

As in the core, different scales are used in different directions to reflect the geometry of the tube. The pressure $\check{P}$ in the boundary layer is scaled in the same way as the oscillatory pressure in the core, so

$$\check{p} = \check{P}. \tag{A 5}$$

The form of the Navier–Stokes equations in general orthogonal curvilinear coordinates is well known (see, e.g. Aris 1962). We now rewrite them using the stretched boundary-layer coordinates introduced above. The continuity equation (2.8*a*) becomes

$$-\frac{1}{\epsilon H_Y H_Z}\frac{\partial}{\partial \check{X}}(H_Y H_Z \check{U}) + \frac{1}{H_Y H_Z}\frac{\partial}{\partial \check{Y}}(H_Z \check{V}) + \frac{1}{H_Y H_Z}\frac{\partial}{\partial \check{Z}}(H_Y \check{W}) = 0. \tag{A 6}$$

Since H_Y and H_Z are independent of $\check{X}$ at leading order, the leading-order components of $\bar{U}$ and $\tilde{U}$ (see (3.6)) are uniform in X. (The different scaling for $\hat{V}$ and $\hat{W}$ in (3.6) means that the same is not true of $\hat{U}$.) In particular, $\tilde{U}$ is equal to the normal boundary motion at leading order.

The momentum equation (2.8*b*) becomes

$$\frac{\partial \check{U}}{\partial \check{t}} + \frac{\epsilon}{\lambda}\left[-\frac{\check{U}}{\epsilon}\frac{\partial \check{U}}{\partial \check{X}} + \frac{\check{V}}{H_Y}\left(\frac{\partial \check{U}}{\partial \check{Y}} - \check{K}_Y \check{V}\right) + \frac{\check{W}}{H_Y}\left(\frac{\partial \check{U}}{\partial \check{Z}} - \check{K}_Z \check{W}\right)\right] = \frac{1}{\epsilon^2 \beta}\frac{\partial \check{P}}{\partial \check{X}} + \frac{1}{R^2}\frac{\partial}{\partial \check{X}}\left(\frac{1}{H_Y H_Z}\frac{\partial}{\partial \check{X}}(H_Y H_Z \check{U})\right) + O(\epsilon^2), \tag{A 7a}$$

$$\frac{\partial \check{V}}{\partial \check{t}} + \frac{\epsilon}{\lambda}\left[-\frac{\check{U}}{\epsilon}\frac{\partial \check{V}}{\partial \check{X}} + \frac{\check{V}}{H_Y}\left(\frac{\partial \check{V}}{\partial \check{Y}} + \check{K}_Y \check{U} + \check{\Gamma}_Y \check{W}\right) + \frac{\check{W}}{H_Z}\left(\frac{\partial \check{V}}{\partial \check{Z}} - \check{\Gamma}_Z \check{W}\right)\right] = -\frac{1}{\epsilon \beta H_Y}\frac{\partial \check{P}}{\partial \check{Y}} + \frac{1}{R^2 H_Z}\frac{\partial}{\partial \check{X}}\left(\frac{H_Z}{H_Y}\frac{\partial}{\partial \check{X}}(H_Y \check{V})\right) + O(\epsilon^2), \tag{A 7b}$$

$$\frac{\partial \check{W}}{\partial t} + \frac{\epsilon}{\lambda}\left[-\frac{\check{U}}{\epsilon}\frac{\partial \check{W}}{\partial \check{X}} + \frac{\check{V}}{H_Y}\left(\frac{\partial \check{W}}{\partial \check{Y}} - \epsilon\beta\, \check{\Gamma}_Y \check{V}\right) + \frac{\check{W}}{H_Z}\left(\frac{\partial \check{W}}{\partial \check{Z}} + \epsilon\beta\, \check{K}_Z U + \epsilon\beta\, \check{\Gamma}_Z \check{V}\right)\right] = -\frac{1}{H_Z}\frac{\partial \check{P}}{\partial \check{Z}} + \frac{1}{R^2 H_Y}\frac{\partial}{\partial \check{X}}\left(\frac{H_Y}{H_Z}\frac{\partial}{\partial \check{X}}(H_Z \check{W})\right) + O(\epsilon^2). \tag{A 7c}$$

The omitted $O(\epsilon^2)$ terms come from the expansion of the Laplacian. We have also made use of the identities

$$\check{\Gamma}_Y \equiv \frac{1}{H_Z}\frac{\partial H_Y}{\partial \check{Z}}, \quad \check{\Gamma}_Z \equiv \frac{\ell^2}{H_Y}\frac{\partial H_Z}{\partial \check{Y}}, \tag{A 8a,b}$$

which can be derived by expanding both sides of

$$\frac{\partial}{\partial Y}(H_Y \hat{\boldsymbol{t}}) \equiv \frac{\partial^2 \boldsymbol{r}}{\partial Y \partial Z} \equiv \frac{\partial}{\partial Z}(H_Z \hat{\boldsymbol{b}}). \tag{A 9}$$

From (A 7*a*), we see that the pressure is uniform across the boundary layer at leading order as $\epsilon \to 0$. Its value will be determined by matching with the pressure in the core.

We decompose the variables in the boundary layer into steady, fundamental, and higher frequency components, as we did for the core; see (3.6). The corresponding decomposition of the equations is straightforward, and we omit the details for brevity.

A.3. *Boundary and matching conditions*

We now translate the various boundary conditions to dimensionless variables and derive the matching conditions between the core and the Stokes boundary layer.

We apply the no-slip condition (2.9) at the material point $(\check{X}', \check{Y}', \check{Z}')$ on the wall that would have been at $(0, \check{Y}, \check{Z})$ in the steady configuration. We obtain

$$\check{U} = \lambda\delta\check{\omega}\mathrm{Re}(\mathrm{i}\xi \mathrm{e}^{\mathrm{i}\check{\omega}\check{t}}), \quad \check{V} = \lambda\delta\check{\omega}\mathrm{Re}(\mathrm{i}\eta \mathrm{e}^{\mathrm{i}\check{\omega}\check{t}}), \quad \check{W} = \lambda\epsilon\delta\beta\check{\omega}\,\mathrm{Re}(\mathrm{i}\zeta \mathrm{e}^{\mathrm{i}\check{\omega}\check{t}}) \qquad (\mathrm{A}\,10a\text{–}c)$$

at

$$\check{X}' = 0 - \delta\,\mathrm{Re}(\xi(\check{Y}, \check{Z})\,\mathrm{e}^{\mathrm{i}\check{\omega}\check{t}}), \qquad (\mathrm{A}\,11a)$$

$$\check{Y}' = \check{Y} + \epsilon\delta\,\mathrm{Re}(\eta(\check{Y}, \check{Z})\,\mathrm{e}^{\mathrm{i}\check{\omega}\check{t}}), \qquad (\mathrm{A}\,11b)$$

$$\check{Z}' = \check{Z} + \epsilon^2\delta\beta\,\mathrm{Re}(\zeta(\check{Y}, \check{Z})\,\mathrm{e}^{\mathrm{i}\check{\omega}\check{t}}). \qquad (\mathrm{A}\,11c)$$

Linearizing to $(\check{X}', \check{Y}', \check{Z}')$ back to $(0, \check{Y}, \check{Z})$, and splitting into frequency components as in (3.1), we obtain

$$\bar{U} = O(\epsilon\delta^2), \quad \tilde{U} = \mathrm{Re}(\mathrm{i}\check{\omega}\xi \mathrm{e}^{\mathrm{i}\check{\omega}\check{t}}) + O(\epsilon\delta^2), \qquad (\mathrm{A}\,12a,b)$$

$$\hat{U} = \frac{1}{\epsilon}\left[\!\left[\mathrm{Re}(\xi \mathrm{e}^{\mathrm{i}\check{\omega}\check{t}})\frac{\partial \tilde{U}}{\partial \check{X}}\right]\!\right]_2 - \left[\!\left[\mathrm{Re}(\eta \mathrm{e}^{\mathrm{i}\check{\omega}\check{t}})\frac{\partial \tilde{U}}{\partial \check{Y}}\right]\!\right]_2 + O(\epsilon), \qquad (\mathrm{A}\,12c)$$

$$\bar{V} = \lambda\delta^2\left[\!\left[\mathrm{Re}(\xi \mathrm{e}^{\mathrm{i}\check{\omega}\check{t}})\frac{\partial \tilde{V}}{\partial \check{X}}\right]\!\right]_0 + O(\epsilon\delta^2), \quad \tilde{V} = \mathrm{Re}(\mathrm{i}\omega\eta \mathrm{e}^{\mathrm{i}\check{\omega}\check{t}}) + O(\epsilon), \qquad (\mathrm{A}\,13a,b)$$

$$\hat{V} = \left[\!\left[\mathrm{Re}(\xi \mathrm{e}^{\mathrm{i}\check{\omega}\check{t}})\frac{\partial \tilde{V}}{\partial \check{X}}\right]\!\right]_2 + O(\epsilon), \qquad (\mathrm{A}\,13c)$$

$$\bar{W} = \lambda\delta^2\left[\!\left[\mathrm{Re}(\xi \mathrm{e}^{\mathrm{i}\check{\omega}\check{t}})\frac{\partial \tilde{W}}{\partial \check{X}}\right]\!\right]_0 + O(\epsilon\delta^2), \quad \tilde{W} = O(\epsilon), \qquad (\mathrm{A}\,14a,b)$$

$$\hat{W} = \left[\!\left[\mathrm{Re}(\xi \mathrm{e}^{\mathrm{i}\check{\omega}\check{t}})\frac{\partial \tilde{W}}{\partial \check{X}}\right]\!\right]_2 + O(\epsilon). \qquad (\mathrm{A}\,14c)$$

Simplifications arise since $\tilde{U}$ and $\bar{U}$ are uniform in $\check{X}$ at leading order, which follows from (A 6) and the fact that the leading-order steady flow does not have a Stokes-layer structure. In particular, we have $\partial\tilde{U}/\partial\check{X} = O(\epsilon)$, so there is no $O(\epsilon^{-1})$ contribution to the condition on $\hat{U}$.

Equations relating the velocity and pressure between the Stokes layer and core region are derived from matching the asymptotic expansions between the two regions (see § 5 of Hinch 1991). We must compare the behaviour of the boundary-layer variables as $\check{X} \to \infty$ with the behaviour of the core variables as $\mathscr{W}$ is approached. We make use of the notation introduced in (3.7) and expand the boundary-layer and core variables about a point $\check{\boldsymbol{x}}_0$ corresponding to the surface coordinates $(\check{Y}_0, \check{Z}_0)$. For the pressure we have

$$\check{p}(\check{\boldsymbol{x}}_0) + (\check{\boldsymbol{x}} - \check{\boldsymbol{x}}_0)\cdot\check{\boldsymbol{\nabla}}\check{p}(\check{\boldsymbol{x}}_0) + \cdots \sim \check{P}^{\infty}(\check{Y}_0, \check{Z}_0) + \check{X}\,\check{P}'^{\infty}(\check{Y}_0, \check{Z}_0) + \cdots, \qquad (\mathrm{A}\,15a)$$

$$\check{\boldsymbol{u}}(\check{\boldsymbol{x}}_0) + (\check{\boldsymbol{x}} - \check{\boldsymbol{x}}_0)\cdot\check{\boldsymbol{\nabla}}\check{\boldsymbol{u}}(\check{\boldsymbol{x}}_0) + \cdots \sim \check{\boldsymbol{U}}^{\infty}(\check{Y}_0, \check{Z}_0) + \check{X}\,\check{\boldsymbol{U}}'^{\infty}(\check{Y}_0, \check{Z}_0) + \cdots, \qquad (\mathrm{A}\,15b)$$

where the coordinates are related by

$$\check{\boldsymbol{x}} - \check{\boldsymbol{x}}_0 = -\epsilon\check{X}\hat{\boldsymbol{n}}. \qquad (\mathrm{A}\,16)$$

We split (A 15) into frequency components and expand both sides in powers of ϵ and δ. Equating coefficients then yields the appropriate matching conditions on the various components.

Appendix B. Boundary-layer and higher-order steady effects

B.1. *The leading-order flow in the Stokes layer*

Following § 7.2, we consider the steady flow in the Stokes-layer region to $O(\delta^2)$. There are $O(\delta^2)$ forcing terms due to the incomplete cancellation between the pressure modification and the Reynolds stress term from the oscillatory flow, and also from the linearization of the boundary condition on the tube wall. However, as shown below, there is no overall effect on the core flow at $O(\delta^2)$.

We expand the variables in powers of δ as in the core, so

$$\bar{\boldsymbol{U}} = \bar{\boldsymbol{U}}_0 + \delta^2 \bar{\boldsymbol{U}}_2 + O(\delta^4), \tag{B 1}$$

$$\bar{P} = \bar{P}_0 + \delta^2 \bar{P}_2 + O(\delta^4). \tag{B 2}$$

At $O(\delta^0)$, there is no specific boundary-layer behaviour. An analysis in the boundary-layer coordinates shows that the boundary-layer flow just mimics the core flow close to the wall and transfers the wall boundary conditions unchanged to the core region.

At $O(\delta^2)$, the steady components of (A 6) and (A 7) are

$$\frac{\partial \bar{U}_2}{\partial \check{X}} = O(\epsilon), \tag{B 3a}$$

$$0 = -\frac{1}{\beta\lambda}\frac{\partial \bar{P}_2}{\partial \check{X}} + O(\epsilon^2), \tag{B 3b}$$

$$-\frac{1}{\lambda}\left(\bar{U}_2\frac{\partial \bar{V}_0}{\partial \check{X}} + \bar{U}_0\frac{\partial \bar{V}_2}{\partial \check{X}}\right) - \frac{\lambda}{2}\,\mathrm{Re}\left(\tilde{U}_{00}^{\dagger}\frac{\partial \tilde{V}_{00}}{\partial \check{X}}\right) = -\frac{1}{\lambda\beta H_Y^s}\frac{\partial \bar{P}_2}{\partial \check{Y}} + \frac{1}{R^2}\frac{\partial^2 \bar{V}_2}{\partial \check{X}^2} + O(\epsilon), \tag{B 3c}$$

$$-\frac{1}{\lambda}\left(\bar{U}_2\frac{\partial \bar{W}_0}{\partial \check{X}} + \bar{U}_0\frac{\partial \bar{W}_2}{\partial \check{X}}\right) - \frac{\lambda}{2}\,\mathrm{Re}\left(\tilde{U}_{00}^{\dagger}\frac{\partial \tilde{W}_{00}}{\partial \check{X}}\right) = \frac{1}{R^2}\frac{\partial^2 \bar{W}_2}{\partial \check{X}^2} + O(\epsilon), \tag{B 3d}$$

where the superscript $\dagger$ denotes the complex conjugate. From (A 12)–(A 14) the boundary conditions at $\check{X} = 0$ are

$$\bar{U}_2 = O(\epsilon), \quad \bar{V}_2 = \frac{\lambda}{2}\mathrm{Re}\left(\xi^{\dagger}\frac{\partial \tilde{V}_{00}}{\partial \check{X}}\right) + O(\epsilon), \quad \bar{W}_2 = \frac{\lambda}{2}\mathrm{Re}\left(\xi^{\dagger}\frac{\partial \tilde{W}_{00}}{\partial \check{X}}\right) + O(\epsilon), \tag{B 4a–c}$$

and from (A 15) the relevant matching conditions as $\check{X} \to \infty$ are

$$\bar{U}_2'^{\infty} = O(\epsilon), \quad \bar{V}_2'^{\infty} = O(\epsilon), \quad \bar{W}_2'^{\infty} = O(\epsilon), \quad \bar{P}_2 \to \bar{P}_2^{\infty} = \bar{p}_2|_{\mathscr{C}}\,. \tag{B 5a–d}$$

Noting that $\nabla_{\perp}\bar{p}_2 = O(\epsilon)$ from (7.3*b*) and $\bar{U}_0 = O(\epsilon)$, and making use of (5.23*c*) and (5.23*d*), we find that the solution to (B 3)–(B 5), to leading order in ϵ, can be written as

$$\bar{U}_2 = O(\epsilon), \quad \bar{V}_2 = \frac{\lambda}{2}\mathrm{Re}\left(\xi^{\dagger}\frac{\partial \tilde{V}_{00}}{\partial \check{X}}\right) + O(\epsilon), \quad \bar{W}_2 = \frac{\lambda}{2}\mathrm{Re}\left(\xi^{\dagger}\frac{\partial \tilde{W}_{00}}{\partial \check{X}}\right) + O(\epsilon), \tag{B 6a–c}$$

$$\bar{P}_2 = \bar{p}_2|_{\mathscr{C}_0} + O(\epsilon). \tag{B 6d}$$

Since $\tilde{V}_{00}'^{\infty} = \tilde{W}_{00}'^{\infty} = 0$, we have

$$\bar{U}_2^{\infty} = O(\epsilon), \quad \bar{V}_2^{\infty} = O(\epsilon), \quad \bar{W}_2^{\infty} = O(\epsilon), \tag{B 7a–c}$$

which confirms the boundary conditions (7.4*d*) assumed above for the core flow.

B.2. *Steady streaming effects in the core*

Beyond leading order, the flow in the core has additional forcing from the matching conditions with the boundary layer. In general, there will be non-zero boundary conditions on both the normal and tangential velocities. The latter is analogous to the classical 'steady streaming' flow that is a typical feature of flows with oscillatory Stokes boundary layers. The effects are not present at leading order and are not readily observable in the numerical computations presented in Part 2 of this paper (Whittaker 2010). We therefore do not investigate this feature further.

REFERENCES

Aris, R. 1962 *Vectors, Tensors, and the Basic Equations of Fluid Mechanics*. Prentice-Hall.

Avrahami, I. D. I. T. & Gharib, M. 2008 Computational studies of resonance wave pumping in compliant tubes. *J. Fluid Mech.* **608**, 139–160.

Bertram, C. D. 2003 Experimental studies of collapsible tubes. In *Flow Past Highly Compliant Boundaries and in Collapsible Tubes* (ed. P. W. Carpenter & T. J. Pedley), chap. 3, pp. 51–65. Kluwer Academic.

Bringley, T. T., Childress, S., Vandenberghe, N. & Zhang, J. 2008 An experimental investigation and a simple model of a valveless pump. *Phys. Fluids* **20**, 033602.

Floryan, J. F. 2003 Vortex instability in a diverging–converging channel. *J. Fluid Mech.* **482**, 17–50.

Floryan, J. F., Szumbarski, J. & Wu, X. 2002 Stability of flow in a channel with vibrating walls. *Phys. Fluids* **14**, 3927–3936.

Gao, P. & Lu, X.-Y. 2006 Instability of channel flow with oscillatory wall suction/blowing. *Phys. Fluids* **18**, 034102.

Grotberg, J. B. & Jensen, O. E. 2004 Biofluid mechanics in flexible tubes. *Annu. Rev. Fluid Mech.* **36**, 121–147.

Heil, M. & Jensen, O. E. 2003 Flows in deformable tubes and channels: theoretical models and biological applications. In *Flow Past Highly Compliant Boundaries and in Collapsible Tubes* (ed. P. W. Carpenter & T. J. Pedley), chap 2, pp. 15–49. Kluwer Academic.

Heil, M. & Waters, S. L. 2006 Transverse flows in rapidly oscillating elastic cylindrical shells. *J. Fluid Mech.* **547**, 185–214.

Heil, M. & Waters, S. L. 2008 How rapidly oscillating collapsible tubes extract energy from a viscous mean flow. *J. Fluid Mech.* **601**, 199–227.

Hickerson, A., Rinderknecht, D. & Gharib, M. 2005 Experimental study of the behaviour of a valveless impedance pump. *Exper. Fluids* **39** (4), 787.

Hickerson, A. I. & Gharib, M. 2006 On the resonance of a pliant tube as a mechanism for valveless pumping. *J. Fluid Mech.* **555**, 141–148.

Hinch, E. J. 1991 *Perturbation Methods*. Cambridge University Press.

Jensen, O. E. & Heil, M. 2003 High-frequency self-excited oscillations on a collapsible-channel flow. *J. Fluid Mech.* **481**, 235–268.

Jovanovic, M. R. 2008 Turbulence suppression in channel flows by small amplitude transverse wall oscillations. *Phys. Fluids* **20**, 014101.

Jovanovic, M. R. & Bamieh, B. 2005 Componentwise energy amplification in channel flows. *J. Fluid Mech.* **534**, 145–183.

Liebau, G. 1954 Über ein ventilloses Pumpprinzip. *Naturwissenschaften* **41**, 327.

Luo, X. Y., Cai, Z., Li, W. G. & Pedley, T. J. 2008 The cascade structure of linear instability in collapsible channel flows. *J. Fluid Mech.* **600**, 45–76.

Luo, X. Y. & Pedley, T. J. 1996 A numerical simulation of unsteady flow in a two-dimensional collapsible channel. *J. Fluid Mech.* **314**, 191–225.

Pedley, T. J. & Stephanoff, K. D. 1985 Flow along a channel with a time-dependent indentation: the generation of vorticity waves. *J. Fluid Mech.* **160**, 337–367.

Ralph, M. E. & Pedley, T. J. 1988 Flow in a channel with a moving indentation. *J. Fluid Mech.* **190**, 87–112.

Smith, F. T. 1976*a* Flow through constricted or dilated pipes and channels. Part 1. *Q. J. Mech. Appl. Math.* **29**, 343–364.

Smith, F. T. 1976*b* Flow through constricted or dilated pipes and channels. Part 2. *Q. J. Mech. Appl. Math.* **29**, 365–376.

Stewart, P. S., Waters, S. L. & Jensen, O. E. 2009 Local and global instabilities of flow in a flexible-walled channel. *Eur. J. Mech.* B. *Fluids* **28** (4), 541–557.

Szumbarski, J. & Floryan, J. M. 2006 Transient disturbance growth in a corrugated channel. *J. Fluid Mech.* **568**, 243–272.

Whittaker, R. J., Heil, M., Boyle, J., Jensen, O. E. & Waters, S. L. 2010 The energetics of flow through a rapidly oscillating tube. Part 2. Application to an elliptical tube. *J. Fluid Mech.* **648**, 123–153.